Path length and sediment transport estimation from DEMs of Difference: a signal processing approach

Lindsay Capito[1], Enrico Pandrin[2], Walter Bertoldi[2], Nicola Surian[1], Simone Bizzi[1]

[1] Department of Geosciences, University of Padova, Padova, 35131, Italy

[2] Department of Civil, Environmental, and Mechanical Engineering, University of Trento, Trento, 38122, Italy

Correspondence to: Lindsay Capito (lindsaymarie.capito@studenti.unipd.it)

Abstract. The difficulties of measuring bedload transport in gravel bed rivers have given rise to the morphological method wherein sediment transport can be inferred from changes in riverbed elevation and estimates of the distance traveled by sediment, its path length. Because current methods for estimating path length are time and labor intensive, we present a method to estimate a characteristic path length from repeat digital elevation models (DEMs of difference i.e., DoDs). We propose an automated method to extract the spacing between erosional and depositional sites on the DoD by the application of Variational Mode Decomposition (VMD), a signal processing method, to quantify the spacing as a proxy for path length. We developed this method using flume experiments where bed topography and sediment flux were measured and then applied it to published field data with physical path length measured from tracer measurements. Our sediment transport estimates were not significantly different than the measured sediment flux at lower discharges in the lab. However, we observed an underestimation of sediment flux at the higher discharges in the flume study. We interpret this as a limit of the method in confined settings, where sediment transport becomes decoupled from morphological changes. We also explore how the time between survey acquisitions, the morphological active width relative to the channel width, and DoD thresholding techniques affect the proposed method and the potential issues they pose to the morphological method in general.

1 Introduction

In gravel bed rivers sediment transport fundamentally controls morphological processes but is notoriously difficult to measure due to its spatial and temporal heterogeneity (Hoey, 1992; McLean and Church, 1999), measurement uncertainty (Vericat et al., 2006), and the logistical challenges of field measurements. The morphological approach is a method to estimate bedload transport based on observed changes in morphology. There have been many implementations of the morphological method since its inception and it has been reviewed extensively (Ashmore and Church, 1998; Brewer and Passmore, 2002; Church, 2006; Vericat et al., 2017). With the increased availability of hydrologic data and modeling capabilities the morphological method has also been applied in two dimensions (x,y) by coupling a 2D hydraulic model to account for sediment routing (Lane et al., 1995; Antoniazza et al., 2019; Bakker et al., 2019). These 2D applications shed light on the functional links between topographic changes and spatial distribution of bedload transport. Antoniazza et al., (2019) quantified the potential errors in estimating sediment transport using with a 1D approach where 2D cross-stream sediment fluxes are neglected.The error associated with neglecting the 2D fluxes which may be especially importantuseful in multithreaded channels. They also explored how DEM accuracy and the frequency of acquisitions affect the estimates of sediment fluxes derived by the morphological method. These 2D apllications contributions confirm the applicability ofenhance the accuracy of the morphological method to estimate sediment transport, however, these studies benefited from they require intensive field campaigns and an accurate accounting of upstream water and sediment supplies, often not available in real case studies. In this paper, the desire is to explore novel approaches to apply the

38   morphological method using topographic data alone, as hydraulic and sediment supply data are not available in many
39   applications and management situations.

40

41   The morphological method can be formalized based on the sediment continuity equation:

42    $$(Q_{b_{in}} - Q_{b_{out}})\Delta t = (1 - p)\Delta V , \tag{1}$$

43   where $Q_{b_{in}}$ and $Q_{b_{out}}$ are the volumetric sediment flux in and out of the reach respectively, Δt is the time between
44   surveys, p is the sediment porosity, and ΔV is the change in volume (Ashmore and Church, 1998; Church, 2006). The
45   sediment continuity equation can be solved in several ways, but in addition to ΔV measured from the DoDs, it requires
46   that either the incoming flux $Q_{b_{in}}$ or the outgoing flux $Q_{b_{out}}$ be defined. In most cases, neither of these fluxes are
47   known, as they are the exact parameters that need to be estimated when applying the morphological method. This
48   conundrum has been addressed by setting a zero-flux boundary, such as a dam or gravel sand transition (McLean and
49   Church, 1999), by segmenting the reach such that a zero-flux boundary is set between a section of net deposition to one
50   of net erosion (Vericat et al., 2017; Calle et al., 2020) or by measuring flux either into or out of the reach (Grams et al.,
51   2013; Antoniazza et al., 2019).

52   Alternatively, Eq. (1) can be modified so that active layer depth, d_s and width w_s ,and the virtual velocity, v_b are used:

53    $$Q_b = v_b \, d_s \, w_s \, (1 - p)\rho_s \tag{2}$$

54

55   Where w_s is the active layer thickness, generally measured by chains and estimated by depth of scour (Church and
56   Haschenburger, 2017), and v_b is equal to $L/T-$, L being the distance the particles travel and T the time over which the
57   particles are traveling (Church, 2006). The virtual velocity approach has been successfully applied using tracer gravels to
58   estimate the path length parameter L in a variety of morphological settings (Liébault et al., 2012; Mao et al., 2017; Brenna
59   et al., 2019, 2020; Brenna and Surian, 2023). Unfortunately, tracer studies are time and labor intensive, requiring multiple
60   site visits and intensive recovery campaigns which often have low recovery rates, especially for painted clasts (Hassan
61   and Bradley, 2017; Brenna et al., 2019). Furthermore, tracer studies are often applicable only to exposed bars, ignoring a
62   large portion of in-channel transport, and can be sensitive to the seeding location (Liébault et al., 2012). To overcome
63   these limitations, several methods have been proposed to estimate path length based on the connection to morphology.

64   The term path length describes the distance traveled by a particle from entrainment to deposition during a transport event
65   and is punctuated by shorter bursts of movement termed step lengths (Einstein, 1937). Individual particles do not all
66   entrain, travel, and deposit together in unison but rather form a distribution of path lengths potentially dependent on grain
67   size, flow strength and duration, and channel morphology. The relative strength of these physical controls on path length
68   has been explored with varied results. Some studies have found relationships between path length and flow metrics such
69   as stream power (Hassan et al., 1992; Schneider et al., 2014; Vázquez-Tarrío and Batalla, 2019; Vázquez-Tarrío et al.,
70   2019) but a considerable scatter in the data has reinvigorated the debate over the role of morphology as a primary control
71   of path length (Hassan and Bradley, 2017; Vázquez-Tarrío and Batalla, 2019; Vázquez-Tarrío et al., 2019).

72   The connection between morphology and path length has long been discussed. Neill (1971) proposed that path length in

73   meandering rivers should be equal to the distance from an erosional site (eroding bank) to the next depositional site (point

74   bar) downstream. Many others have observed similar relationships based on the spacing of erosional and depositional

75   sites and channel morphology (Beechie, 2001; Pyrce and Ashmore, 2003a, b; Hundey and Ashmore, 2009; Kasprak et

76   al., 2015; Vázquez-Tarrío et al., 2019). Further, depositional areas (typically bars), have demonstrated a higher probability

77   of 'trapping' particles than erosional morphological units (McDowell and Hassan, 2020; McDowell et al., 2021). Finally,

78   experimental research has confirmed the preferential deposition of particles specifically at bar heads and margins even in

79   channels with more complex morphology, for example, in braided rivers (Kasprak et al., 2015) but it is reasonable to

80   assume that in multithreaded channels, multiple path lengths might exist at different flow stages in primary and secondary

81   channels.

82   The path length used for the virtual velocity approach is generally taken as the mean travel distance (Wilcock, 1997;

83   Vericat et al., 2017; Mao et al., 2017; Brenna et al., 2019). However, as we have seen from tracer studies, particles tend

84   to form a distribution of travel distances, therefore, it is unclear if the mean path length ~~as measured by tracers~~ is the best

85   representation of a 'characteristic' path length to estimate bedload transport. To obtain an estimate of reach scale sediment

86   transport we want to approximate~~consider~~ the distance travelled by the bedload ~~involved in~~that build~~sing~~ geomorphic

87   units, this is what we will consider as ~~representative~~ a 'characteristic path length'. Tracer studies have allowed us to see

88   that t~~T~~his may not necessarily be the average distance, as evidenced by the wide variety of path length distributions, it is

89   often the case that many or even most (the mode) of path lengths are very short, thus skewing the average depending on

90   the distribution. For example, Pyrce and Ashmore published synthesis of tracer studies and demonstrated that at formative

91   discharges, particle path length distributions often exhibit primary or secondary modes corresponding to the location of

92   bars, where deposition occurs (Pyrce and Ashmore, 2003a). Further, flume experiments with tracers showed that the

93   majority of particles eroded from an upstream scour pool were deposited at the point bar apex and corresponded to peaks

94   in bi or multimodal path length distributions (Pyrce and Ashmore, 2005). Therefore, the characteristic path length, i.e.,

95   the most representative and sound value to be used in sediment transport estimations, might be better described by these

96   primary or secondary modes in channels with bar morphology at channel forming flows.

97   If a characteristic path length can be inferred from changes in morphology as previously discussed, advances in

98   topographic survey techniques to acquire detailed digital elevation models (DEMs) and facilitate change detection,

99   provide an opportunity to streamline the estimation of sediment transport. The high-resolution topography (HRT)

100 revolution (Vericat et al., 2017) has provided an abundance of high quality surveys and an increased frequency of

101 change detection based on the differencing of DEMs to create digital elevation models of difference (DoDs)

102 (Brasington et al., 2000; Lane et al., 2003). Vericat et al. (2017) proposed an equation to use the path length with the

103 volume of erosion derived directly from the DoD

104
$$Q_b = (v_b \ \sum V_e \ (1-p)\rho_s \,)/L_c \,, \tag{3}$$

105 where $\sum V_e$ is the total volume of erosion from the DoD and L_c is the length of the analyzed DEM by which the volume

106 of erosion is normalized (Vericat et al., 2017). To use this method, L_c must be long enough for average path lengths (L)

107 to occur and T must be short enough to prevent repeated erosion and deposition, known as compensation (Lindsay and

108 Ashmore, 2002).

109 Redolfi (2014) attempted to estimate the path length parameter directly from the DoD using the length of individual

110 erosional patches as a proxy for the length of the erosion-deposition sequence. This approach avoids the need to couple

111 each erosional area to a downstream depositional area, which can be difficult to automate in multi-thread rivers. While

112 this method scales well with flow metrics and provides reasonable estimates (Redolfi, 2014; Vericat et al., 2017), the

113 hypothesis that the length of erosional areas is equivalent to the erosion-deposition distance has not been tested in

114 different morphologies, and it is not clear how the survey resolution may affect the estimates by fragmenting the

115 erosional areas into smaller parts. Recently, Calle et al. (2020) used a method of river segmentation to visualize the

116 pattern of erosion and deposition and infer sediment connectivity as well as to estimate potential travel distances. They

117 defined boundaries between river segments and classified them into types based on their net erosional or depositional

118 characteristics. Focusing on the "type 1 depositional boundary" wherein the upstream section is erosional and the

119 immediate downstream boundary is depositional and depending on the volumes of deposition and erosion in these

120 segments they were able to estimate minimum or maximum transport distances (Calle et al., 2020). This approach

121 provides greater insight into the spatial connectivity of the river corridor and is useful to understand reach scale

122 processes. However, depending on the river, and the sections surveyed, the number of type 1 boundaries may limit the

123 applicability of the method in defining a characteristic path length and crucial information may be missed where the

124 pattern of erosion and deposition is not clear, or the periodicity spans multiple sections. For example, where there are

125 back-to-back patches of erosion or deposition or the overall pattern is separated by small areas of mixed boundaries.

126 Given the observations linking path length to morphology and building on the aforementioned methods, we seek to

127 expand on the idea that characteristic path length can be inferred from changes in morphology at near transport event

128 scale comparisons. If during a flood, sediment is mobilized from an area of erosion to an area of deposition as

129 represented on the DoD, the distance between the two should correspond to a characteristic path length. Following these

130 assumptions this work has the following objectives: i) to propose an objective and semiautomatic method to quantify a

131 characteristic path length as represented by the periodic nature of erosion and deposition from the DoD using flume

132 data; ii) to compare these estimates of a characteristic path length to measured path length distributions obtained from

133 tracer data in the field; iii) and finally to evaluate the conditions in which a characteristic path length is appropriate to

134 estimate sediment transport.

135

2 Methods

137 To meet our objectives, we use flume experiments at varying discharges with direct measurement of output sediment flux

138 and sets of repeat DEMs from which DoDs are created and used to identify patterns of erosion and deposition. We then

139 develop a semiautomated method to extract these distances between erosion and deposition as a proxy for the

140 characteristic path length and then compare our estimates of sediment flux calculated using the characteristic path length

141 to measured sediment flux. Finally, we compare the characteristic path length estimates from a published case study to

142 the physical path length distributions as measured by tracers in the field to see how the characteristic path length

143 corresponds to path length distributions.

144

2.1 Path length

146

147 A key assumption inherent in our objectives is that sediment moves from an area of net erosion to an area of net

148 deposition during the time period between DEM acquisitions and that this represents a characteristic path length.

149 Ferguson and Ashworth (1992) proposed a similar method of matching specific erosional and depositional patches

150 albeit without the assistance of a DoD. This method was then implemented in the Sunwapta River, Canada (Goff and

151 Ashmore, 1994) although the authors note the difficulty in finding perfectly matching patches and conclude that

152 erosional and depositional processes are likely more dispersed. Here we will implement this "manual method" as a

153 means of comparison for the automated method presented later. The most obvious method to quantify this distance

154 between erosional and depositional sites on the DoD is to measure the spacing manually using a GIS program however,

155 this requires many subjective evaluations. Firstly, we must decide where on the patches of erosion and deposition to

156 begin and end the measurements. Because patches of erosion and deposition are not symmetrical or of equal size, the

157 distance between the two depends on which area of the patch we choose to begin and end the measurements. For

158 consistency, we choose the center of the patch (Fig. 1) after Ashmore and Church (1998). Next, we must determine

159 which patch of erosion matches with which patch of deposition which is not always obvious, and as noted previously,

160 likely does not accurately represent the nature of bedload transport (Goff and Ashmore, 1994). Here we perform this

161 method solely for comparative purposes and therefore used our knowledge of morphological processes to make a best

162 estimate. For example, a patch of erosion on an outside bend likely corresponds to the deposition of the next point bar

163 downstream (Fig. 1). Although this method is capable of producing crude estimates of path length to overcome the

164 aforementioned biases (Ferguson and Ashworth, 1992; Goff and Ashmore, 1994; Ashmore and Church, 1998) we

165 propose a method to estimate a characteristic path length without relying on the matching of erosion and deposition but

166 rather to use the periodic nature of these processes. Additionally, we seek to create a method that is both objective and

167 semiautomated.
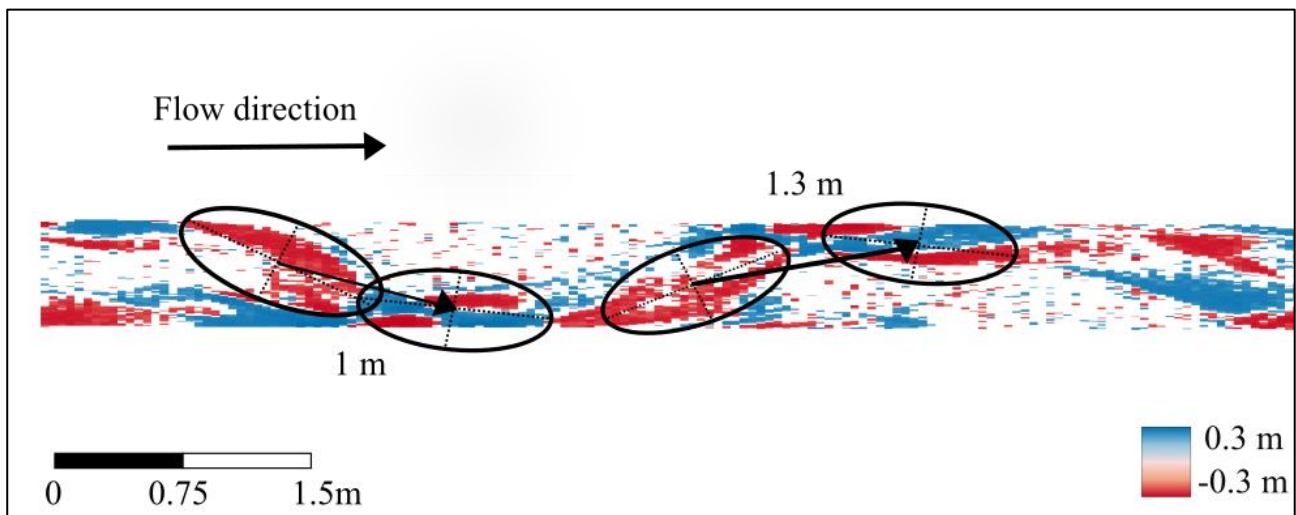
169 **Figure 1: Manual method to measure spacing of erosional patches (red) and depositional patches (blue) on a**
170 **DoD.**

171

172 **2.2 Semiautomated extraction of path length**
173 To visualize and then quantify the periodic nature of erosion and deposition from the DoD we simplify the spatial

174 heterogeneity of the DoD into a vector of the net change in elevation in a streamwise direction (Fig. 2a). Because

175 natural rivers are rarely straight, for field case studies, we must enforce a linear downstream directionality essentially

176 straightening the bends in the river. This is achieved by segmenting the DoD into a series of equally sized "bins" using

177 the segmentation tool of the Fluvial Corridor Toolbox (Roux et al., 2015) (Fig. 2a). The bin size can affect the pattern of

178 erosion and deposition in that by selecting too large of bins we may miss important erosional or depositional areas when

179 they are summed in the same bin. Similar methods that require river segmentation have proposed using the reach

180 averaged width for the length of the bins (McDowell et al., 2021) or half of the width of the reach (McDowell and

181 Hassan, 2020) although these studies had different objectives. Calle et al. (2020) applied a segmentation method with a

182 similar goal of identifying corresponding zones of erosion and deposition and set the bin sized based an assessment of

183 the river dimensions as well as the minimum transfer distance of interest. Therefore, depending on the river, the user

184 may select differently sized bins. Once the river is segmented, we then sum the values in each bin to obtain a vector of

185 the net change in elevation in a downstream direction (Fig. 2b). In the flume studies, where there is no sinuosity, we

186 simply sum each cross section of the DoD matrix. Oftentimes a reach is aggrading or incising and therefore the net

187 vector will have an increasing or decreasing trend (Fig. 2b). Because we are interested in the spacing between areas of

188 erosion and deposition rather than the overall trend, we remove it by subtracting a best-fit linear trend from the net

189 vector (Fig. 2b). Because we simplify the heterogeneity of erosion and deposition into a net vector of elevation change,

190 we risk compensating erosion and deposition within the same cross section, therefore we also create a vector of just

191 erosion and one of just deposition as well as the net allowing for a visual comparison of the relative contribution of

192 erosion and deposition to the net as well as the periodicity of the individual processes (Fig. A1). We can see that there

193 appears to be a periodicity as the net vector oscillates forming peaks and troughs and although this periodicity seems

194 apparent, quantifying the distance is not straightforward.
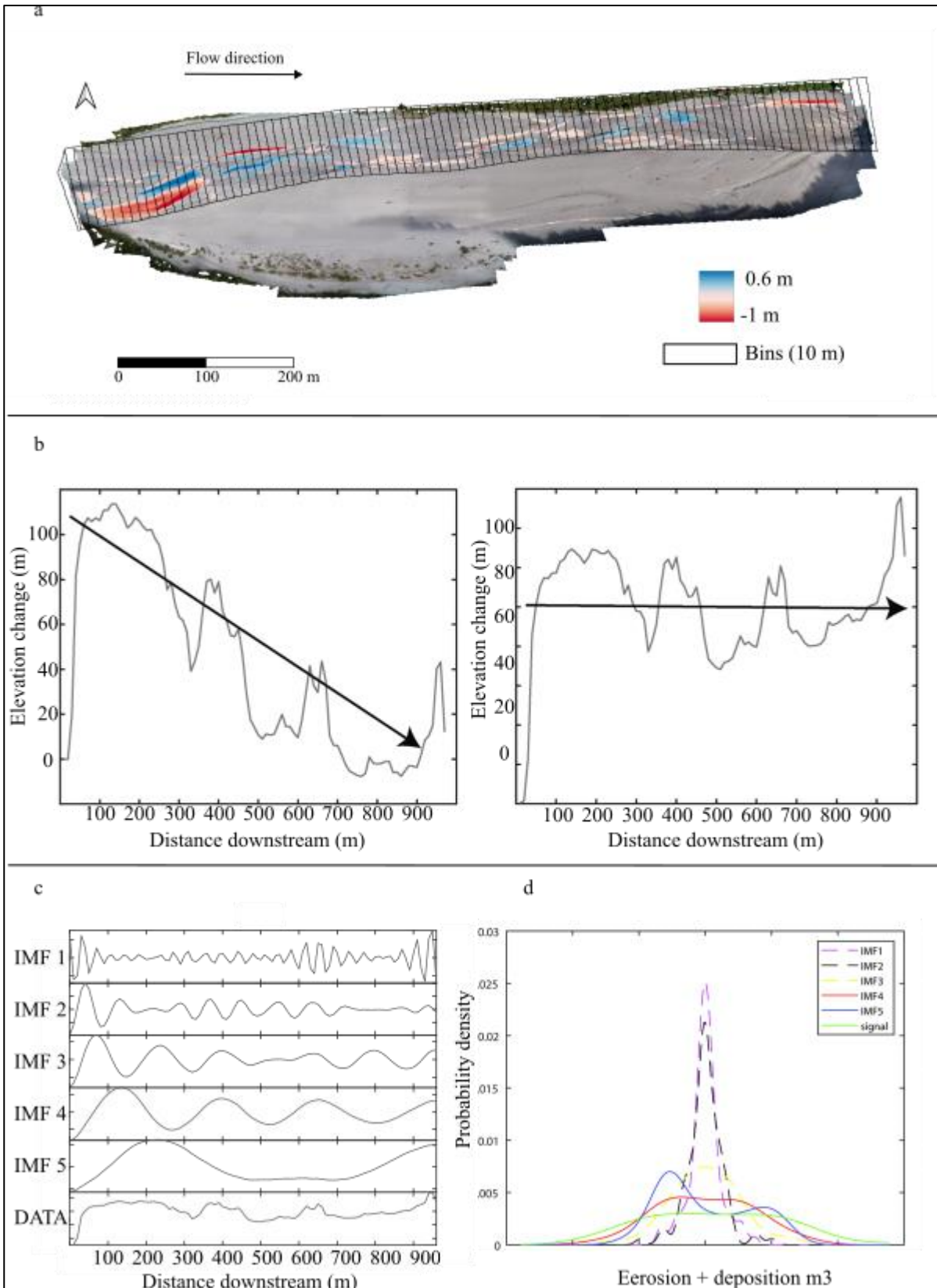
Figure 2: VMD- HD method (a) Segmentation of the DoD (example orthophoto and DoD from the Tagliamento River, Italy). (b) Plot of the net original and detrended vector. (c) Variational mode decomposition (VMD) with 5 intrinsic mode functions (IMFs). (d) Probability density function (PDF) of each IMF and the original net vector.

One approach could be to count the zero crossings and then use that distance as the proxy for path length. However, we risk measuring low magnitude spikes that cross zero that may not necessarily represent the overall periodicity or large

201   oscillations that don't cross the zero line. A smoothing filter may be used to remove these low magnitude oscillations

202   but we risk losing potentially relevant information. To solve this problem, we turn to the realm of signal processing

203   where the practice of "denoising" and extracting information from oscillations is ubiquitous.

204   Signal processing is a field that deals regularly with extracting information and patterns that are not visually apparent

205   and its applications have been used in a wide variety of settings including voice recognition (Sigmund, 2003; Upadhyay

206   and Pachori, 2015), medical applications (Boudraa et al., 2005; Liu et al., 2008), and even time series analysis of

207   climate data (Barnhart and Eichinger, 2011). There are many approaches to de-noising including Fast Fourier transform,

208   empirical mode decomposition (EMD), and wavelet analysis. Each of these methods come with inherent strengths and

209   weaknesses, for example wavelet analysis requires that a mother wavelet be selected a priori and may influence the

210   results (Boudraa et al., 2005). We chose to use variational mode decomposition (VMD) due to its robustness with

211   respect to sampling and noise and the ability to handle signals that exhibit non-linearity and non-stationarity

212   (Dragomiretskiy and Zosso, 2014; Huang et al., 2016; Ma et al., 2017). VMD decomposes the signal into a set of

213   intrinsic mode functions (IMFs) each with a different central frequency (Dragomiretskiy and Zosso, 2014; Ma et al.,

214   2017) (Fig. 2c). In this case of our static 'signal' the frequency is more accurately described as the wavelength. It is

215   beyond the scope of this paper to describe the mathematics of VMD in detail, therefore, for a complete explanation see

216   (Dragomiretskiy and Zosso, 2014; Huang et al., 2016; Ma et al., 2017; Upadhyay and Pachori, 2015).

217   Once the original net vector of erosion and deposition is decomposed into the various IMFs, we need to select the IMF

218   or IMFs that most accurately represent the periodicity of the original data and therefore our characteristic path length.

219   Ma et al. (2017) proposed a method to select the most relevant IMF, and therefore periodicity of the signal, by

220   computing the probability density function (PDF) using kernel density smoothing for each of the five IMFs and of the

221   original data vector (Fig. 2d), then to calculate the Hausdorff distance (HD), a metric of geometric similarity, between

222   each IMF's PDF and the PDF of the original data and select the IMF most geometrically similar to the original data (Ma

223   et al., 2017) (hereafter VMD-HD method). In most cases, the longer wavelength IMFs most closely resemble the

224   original signal whereas the IMFs with shorter wavelengths are more likely associated with noise (Boudraa et al., 2005).

225   The computed wavelength is converted to a meaningful physical quantity by multiplying by the bin spacing in meters.

226   Because we are interested in the distance from peak to trough, we divide the period by two to obtain the path length

227   proxy (Neill, 1971; Ashmore and Church, 1998). Although this method allows for the selection of one IMF to

228   presumably represent the periodicity of the data, we record path lengths calculated from the other IMFs to evaluate the

229   range of estimates generated by the decomposition and determine if the VMD-HD method is appropriate for

230   determining a characteristic path length and the relative importance of other IMFs. All calculations were performed in

231   MatLabR2020b using the built in VMD function and the Hausdorff distance function (Danziger, 2023).

232   One important consideration when using VMD to decompose a signal is that is the user must define the number of IMFs

233   beforehand. The number of IMFs is important as under binning, choosing too few IMFs, may mean that critical IMFs

234   are missed, whereas over binning, can cause duplication of components (Wu et al., 2020). In signal processing, there are

235   sophisticated methods for determining the number of IMFs, for a summary see (Wu et al., 2020). However, for our

236   purposes and simplicity's sake, we performed a brief sensitivity analysis based on the property of convergence often

237   used in the signal processing methods (Wu et al., 2020; Huang et al., 2016; Ma et al., 2017). The default setting in the

238   MatLab function is 5 IMFs, we used 3, 5, 8, 15, and 25 IMFs to calculate path length and assessed how it changed for

239   the maximum IMF (Fig. A2). We found that using more IMFs generally increased the number of high frequency

240   components rather than the lower frequency IMFs (Fig. A3). Because these higher frequencies are generally associated

241 with noise and in our case are physically too small to likely represent meaningful path lengths (on the order of

242 millimeters) we decided more than 5 IMFs did not contribute physically meaningful information in that the IMFs with

243 longer wavelengths did not change drastically. We also determined that 3 IMFs were too few as it was clear that the

244 longer wavelengths were missing (Fig. A3). Therefore, we chose to use the default 5 IMFs as this provided a

245 manageable number of components while effectively separating the lower frequencies. This is a convenient starting

246 point for assessing the VMD method as a tool to extract the periodicity as a proxy for characteristic path length but is by

247 no means the only option. We encourage further exploration of the IMF parameter in future applications and as the

248 method is refined.

249 **3 Flume and field data**

250 The method was tested using data from a set of flume runs performed in the Hydraulic Laboratory of the University of

251 Trento, where DEMs were generated for fixed time intervals and varying discharges, and direct measurements of the

252 bedload flux were also collected. To test the efficacy of the method in the field, we selected a published dataset of

253 measured path lengths with corresponding DoDs for the San Juan River in British Columbia Canada (McQueen et al.,

254 2021). Although McQueen et al. deployed tracers in four separate periods, there was only one deployment (2018-2019)

255 with corresponding DEMs (McQueen et al., 2021). DoDs and corresponding tracer data were available for three

256 separate sites (bar 6, bar 7, and bar 15) for the 2018-2019 period. Detailed information on their collection and

257 processing can be found in McQueen et al., 2021.

258 **3.1 Flume experiments**

259 The Trento laboratory experiments were carried out in a 0.6 m wide and 24 m long flume, filled with nearly uniform 1

260 mm diameter sand. The flume slope was set to 0.01 m/m. Topographic surveys were performed over the final 14 m of

261 the flume, to limit the upstream inflow effects, using a laser gauge, mounted on a movable deck. The longitudinal and

262 crosswise spacings were 0.05 m and 0.005 m, respectively. Four sets of nine runs were performed, with the flow

263 discharge set to 0.7, 1, 1.5, and 2 l/s, which correspond to a range of different planform morphologies (Table 1).

264 Sediment input at the upstream end of the flume was constant in each run, with a flux equal to the average measured at

265 the downstream end, as computed in a preliminary set of experiments. Therefore, the overall average bed elevation of

266 the runs was in equilibrium, with no net erosion or deposition. The runs were performed following the same procedure,

267 involving three phases of different lengths, based on the transport condition of each discharge. These durations were

268 estimated referring to the time scale for morphological evolution computed from the sediment balance mass equation

269 (Garcia Lugo et al., 2015), which can be expressed as:

270
$$T\_ex = \frac{DW^2}{Q_b},$$
(4)

271 where D is the average flow depth and W is the flow width. Table 1 provides the values of T_ex for each flume

272 experiment.

273 **Table 1: Initial conditions for each dataset including the type of validation data.**

	Flume 1	Flume 2	Flume 3	Flume 4	San Juan Bar 6	San Juan Bar 7	San Juan Bar 15
Peak discharge (m³/s)	0.0007	0.001	0.0015	0.002	942	942	942
Slope (m/m)	0.01	0.01	0.01	0.01	0.0038	0.0031	0.0009
Width (m)	0.6	0.6	0.6	0.6	150	150	130

D_{50} (m)	0.001	0.001	0.001	0.001	0.05	0.056	0.042
Time scale T_ex (min) (eq.4)	94	50	38	30	-	-	-
Time between surveys (min)	47	25	19	15	~1 year	~1 year	~1 year
ω* Dimensionless stream power	0.15	0.22	0.33	0.43	0.76	0.61	0.31
Validation Data	Sediment Flux	Sediment Flux	Sediment Flux	Sediment Flux	RFID tracers	RFID tracers	RFID tracers
Planform	Wandering	Wandering	Wandering transitional	Alternate bar	Wandering	Wandering	Wandering

274

275   First, an initial phase of about 12 times this time scale T_ex with constant flow was run, to ensure the formation of a

276   near-equilibrium morphological condition, starting from a flat sand bed scraped to the prescribed slope. This was

277   followed by a long run, at constant discharge, lasting 19 times the time scale T_ex, aimed at measuring the output

278   sediment flux. This was continuously monitored at the channel outlet, through a permeable basket placed on four load

279   cells. Sediment flux was measured every minute. After a bed topography survey, the third phase was a sequence of nine

280   shorter runs, lasting 0.5 times the time scale T_ex, each followed by a bed topography survey, which produced nine

281   corresponding DoDs. The duration of these nine runs (and therefore the time interval between surveys) was decided to

282   have easily measurable changes of the bed morphology, without having significant compensation processes.

283   The DoDs were created by subtracting two consecutive DEMs, then underwent a three-step filtering process to highlight

284   the relevant erosion and deposition patterns, removing most of the noise associated with the surface roughness and

285   measurement accuracy. First, the DoDs were filtered considering a uniform detection threshold equal to 2 mm (2 times

286   the D_{50}), meaning that erosion or deposition values lower than this threshold are set to zero. Thereafter, a spatial average

287   was performed as a moving average on three values along the transversal direction where the DoD discretization is the

288   finest. Lastly, a despeckling algorithm removed all isolated cells, both considering single cells that show erosion or

289   deposition, as well as single cells that show no change. This last step was implemented to keep the detection threshold

290   as low as possible while removing unphysically small areas. Additionally, we calculated the morphological active width

291   by determining the percentage of the DoD that showed morphological activity (i.e., was not zero after filtering).

3.2 San Juan River data

293   To compare the characteristic path length to measured path length distributions in the field, we used data from the San

294   Juan River, located on Vancouver Island, British Columbia with a drainage area of approximately 730 km^2 and a mainly

295   rainfall driven hydrology (McQueen et al., 2021). The reach of interest in this study was alluvial in nature with a

296   wandering morphology and a substrate composed of gravel, cobble, and sand (McQueen et al., 2021). The time in

297   between acquisitions is one year, in which it is estimated there were five flood events able to generate sediment

298   transport using a threshold of 500 m3 s−1, which was visually estimated by the authors to be equivalent to the bankfull

299   discharge (McQueen et al., 2021). DEMs were generated by LiDAR acquisitions and have a spatial resolution of 10 cm

300   and a vertical root mean square error lower than 10 cm. Topographic changes between survey dates were then

301   calculated by processing the LiDAR DEMs using the Geomorphic Change Detection (GCD) software (Wheaton et al.,

302   2010). More information on how they were obtained and processed including the spatially variable thresholding

303   techniques can be found in McQueen et al. (2021). The LiDAR-derived DoDs were used to interpret patterns of tracer

304   displacement and burial depths and to provide information on the morphological development of the bars during the

305   study period. However, they do not provide complete reach-scale sediment budgets due to the lack of in-channel

306 topographic data and stage differences during each LiDAR survey affecting the relative portion of the river bed that was

307 exposed. The submerged area represented 22% of the DoD for bar 6, 42% for bar 7, and 36% for bar 15. Nevertheless,

308 we believe the exposed part of the channel, the bars, and associated patches of erosion and deposition (see Fig. 9b) are

309 sufficient to be used with our proposed method to estimate path lengths and be compared with field measured path

310 lengths from the tracer data as a first application to field data. This is because we are not calculating sediment flux for

311 the San Juan River and are only interested in comparing our estimates of the characteristic path length to the measured

312 tracer distributions. As far as the pattern of erosion and deposition and how that may be disrupted, we recognize that

313 believe that because the submerged area is small relative to the DoD the pattern should notcould change by including

314 the underwater areas, however drastically. Further, by looking at figures 15 and 16 from McQueen et al. (2021) we can

315 see that the tracers were largely recovered from the exposed bar surfaces in the 2018-2019 deployment. This gives us

316 confidence that the deposition we are measuring corresponds largely to the deposition associated with the tracers.

317 Although this is not an ideal situation, we believe the benefits outweigh the limitations considering the difficulty of

318 finding high quality RFID tracer data and corresponding DoDs. The San Juan River DoDs were downloaded directly

319 from the Scholars Portal Dataverse (https://doi.org/10.5683/SP2/UQGZCG). The DoDs were segmented using similar

320 principles to Calle et al. (2020) in a similarly sized river, therefore the bin size was conservatively set at 10 m.

321 **3.3 Validation and error estimation**

322

323 Each study had unique initial conditions including slope, discharge, grain size, channel configurations, and time/flood

324 events between surveys (Table 1). Because the studies vary with respect to these initial conditions, we calculated the

325 dimensionless stream power (ω^*) after Bertoldi et al. (2009) to compare them as:

326
$$\omega^* = \frac{Q \cdot S}{W \sqrt{g \Delta D_{50}^3}}, \tag{5}$$

327 where Q is the peak discharge, S is slope, W is the average wetted width, Δ is the relative submerged density, D_{50} is the

328 median grain size, and g is the acceleration due to gravity.

329 For the flumes, we used estimates of path length generated by the VMD-HD method and those associated with the two

330 longest wavelengths, IMF 4 and IMF 5 separately to calculate the virtual velocity Eq. (2) and sediment flux Eq. (3)

331 which we then compared to measured flux data. The measured sediment flux during the initial long run showed high

332 variability, with phases of high and low sediment flux lasting several tens of minutes. For this reason, we prefer to use

333 the data from the long runs, from which we estimated an average sediment flux of 0.33 g/s (SD=0.17) for the 0.7 l/s

334 discharge, 0.78 g/s (SD=0.31) for the 1 l/s discharge, 1.98 g/s (SD=0.65) for the 1.5 l/s discharge, and 3.22 g/s

335 (SD=0.79) for the 2 l/s discharge. We subdivided the second phase into 38 intervals of 0.5 T_ex duration, equal to the

336 duration as the short runs in phase 3, and computed the variability of the flux over this range.

337 We used ANOVA to compare path length, virtual velocity, and erosion across the four discharges ($\alpha=0.05$) and a Post-

338 hoc Tukey test to explore significant differences between discharges. To compare the measured sediment flux to the

339 estimates from the VMD-HD method and the IMF 4 and IMF 5 estimates we used a student's t-test ($\alpha=0.05$). And

340 finally, to compare the error of our path length and sediment transport estimates we calculated the relative percent error

341 δ in order to compare the sediment flux estimates to that of the long runs of average sediment flux as:

342
$$\delta = \frac{|E - M|}{M}, \tag{6}$$

343 where E is the average of the estimated sediment flux for the 9 runs at a given discharge and M is the averaged

344 measured sediment flux from the long run at the same given discharge. For the San Juan River we compared the VMD-

345 HD estimates of path length and IMFs 4 and 5 qualitatively to the published path length distributions and the locations

346 of mean, median, and modes. The tracer recovery locations were accessed in spreadsheet form and in keeping with the

347 analysis of the authors we disregarded any tracers that moved less than 10 m before calculating the path length

348 distributions.

349 **4 Results**

350 **4.1 Flume experiment**

351 To aid in the interpretation of the results, Fig. 3 shows a DoD from the lowest discharge, 0.7 l/s (a) and the highest

352 discharge, 2 l/s (b) with the net vector (continuous line), IMF 4 (dashed line), and IMF 5 (dotted line) as obtained from

353 the VMD method. Oftentimes the areas of deposition and erosion from the DoD correspond clearly to the IMF 4 and 5

354 vectors as with the 0.7 l/s discharge where areas of deposition are concave and areas of net erosion correspond to

355 convex areas of the vector (Fig. 3a). At the higher discharges (1.5 l/s and 2 l/s) the total area of morphological activity

356 increases and patches of erosion and deposition begin to overlap, creating a more chaotic and difficult to discern pattern

357 (Fig. 3b, A1). We also observed a similar periodicity in the erosional and depositional vectors and at the 2 l/s discharge

358 the depositional vector appears to show this most clearly (Fig. A1).
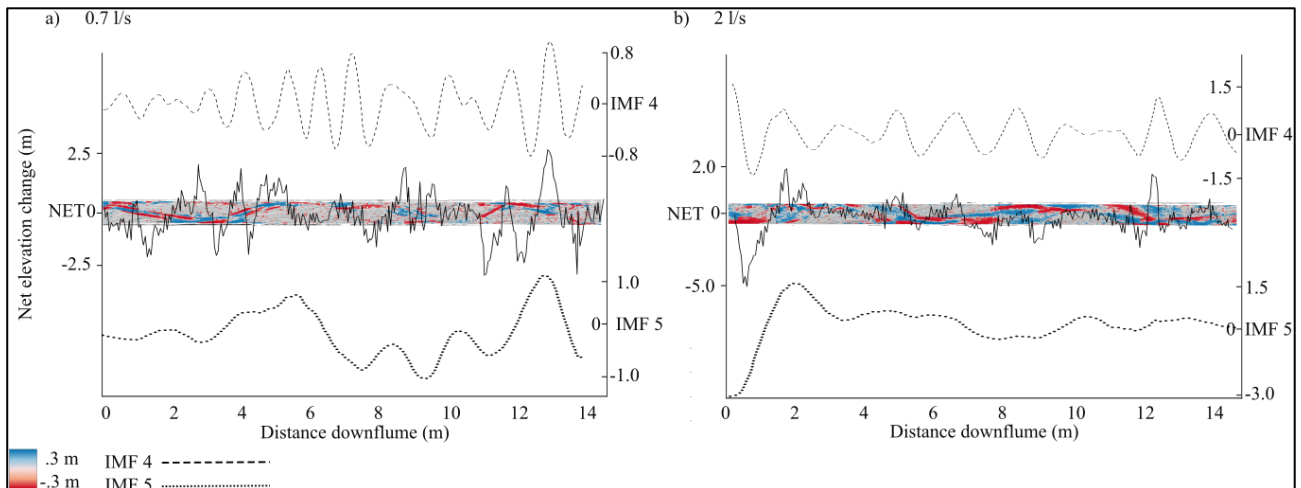
359

360 **Figure 3: DoDs from 0.7 l/s discharge (a) and 2 l/s discharge (b) with the net vector of elevation change laid over**
361 **the top. IMF 4 vector (above, dashed line) and IMF 5 vector (below, dotted line)**

362 In the flume experiment, the VMD-HD method of choosing the most relevant IMF selected the longest wavelength IMF

363 5 71% of the time and IMF 4 23% of the time. IMFs 2 and 3 were never selected and IMF 1 was selected only twice.

364 However, at the higher discharges (1.5 l/s and 2 l/s) IMF 4 was selected more frequently, thereby reducing the average

365 path length when compared to the lower discharges (Fig. A4). Using the selected IMFs, the VMD-HD method

366 estimated a similar average path length for all of the discharges (Fig. 4). The averages were, 1.45 m (standard deviation

367 (SD) = 0.93) for the 0.7 l/s discharge runs, 1.24 m (SD=0.58) for the 1 l/s runs, 1.21 m (SD = 0.58) for the 1.5 l/s runs,

368 and 1 m (SD = 0.37) for the 2 l/s runs (Fig. 4). The path length estimates derived from IMF 4 were similar for all

369 discharges, 0.51 m (SD=0.12) for the 0.7 l/s discharge, 0.55 m (SD=0.16) for the 1 l/s discharge, 0.56 m (SD=0.91) at

370 the 1.5 l/s discharge, and 0.46 m (SD=0.15) at 2 l/s (Fig.4) with no significant differences between the discharges (p >

371 0.05). The path lengths derived from IMF 5 were also similar between the discharges with no significant differences (p

372 > 0.05) and were, 1.75 m (SD=0.79) for the 0.7 l/s discharge, 1.55 m (SD=0.24) for the 1 l/s discharge, 1.79 m

373 (SD=0.67) for the 1.5 l/s discharge, and 1.37 m (SD=0.39) for the 2 l/s discharge (Fig. 4). The VMD-HD method

374 matched closely with the manually measured distances and there were no statistically significant differences for any of

375 the discharges (p-value > 0.05) (Fig. 4) while the IMF 4 and IMF 5 derived path lengths bracket the manually measured

376 distances and the VMD-HD selected path lengths (Fig. 4).
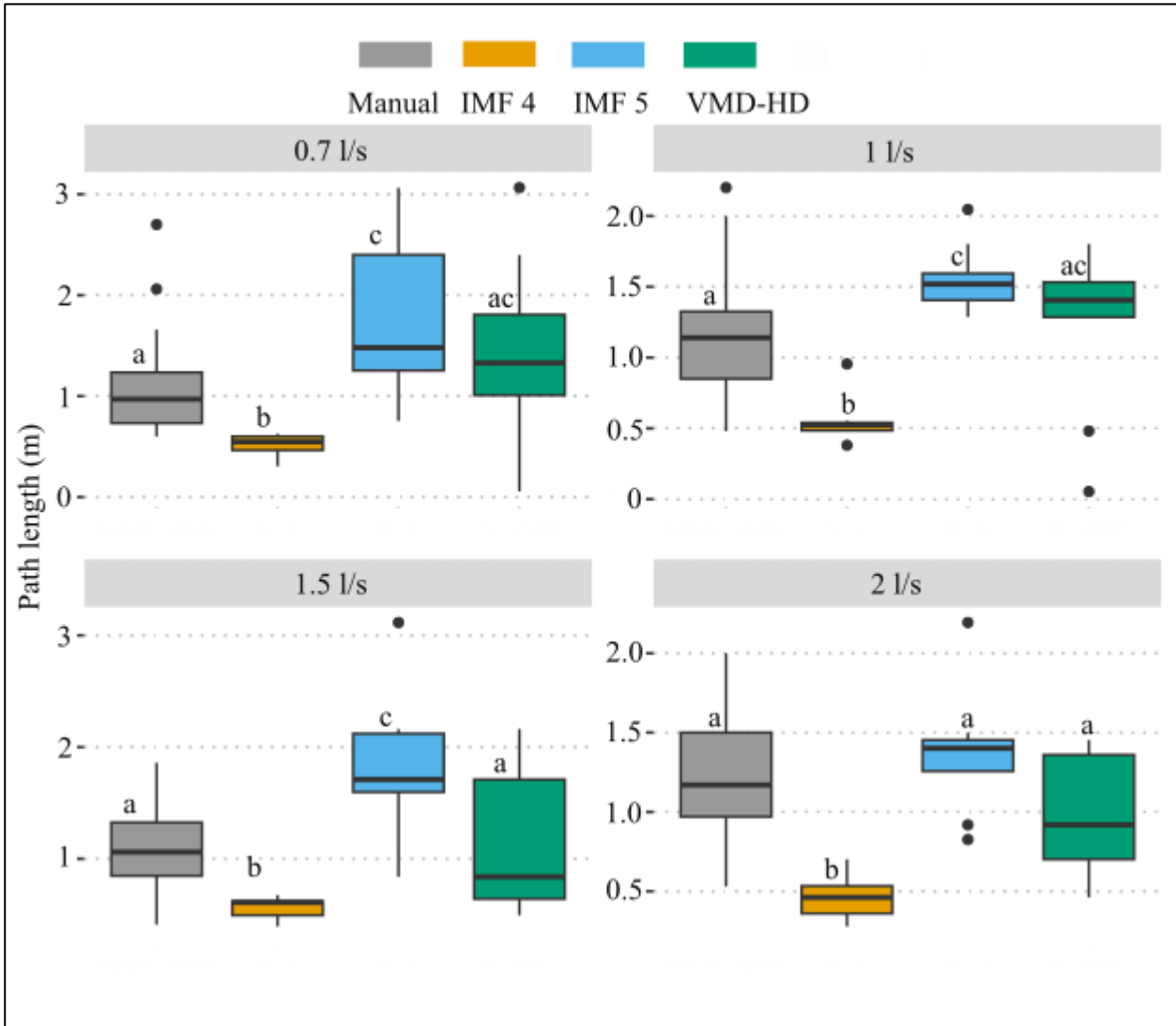
Figure 4: Path length estimates from the manual method (gray), IMF 4 (orange), IMF 5 (blue), and the VMD-HD method (green). Significant differences from the post-hoc Tukey test are denoted by letters a-c.

380 The estimated path lengths were not significantly different between the discharges (p-value >0.05) and showed no

381 obvious trend of increasing or decreasing with discharge. However, when used to calculate the virtual velocity (v_b)

382 wherein the path length is divided by the time between surveys (Table 1), we see an increase in the virtual velocity with

383 discharge (p-value < 0.05) (Fig. 5). Likewise, the average volumes of erosion and deposition calculated from the filtered

384 DoDs increases significantly with discharge (p-value < 0.001) (Fig. 5).
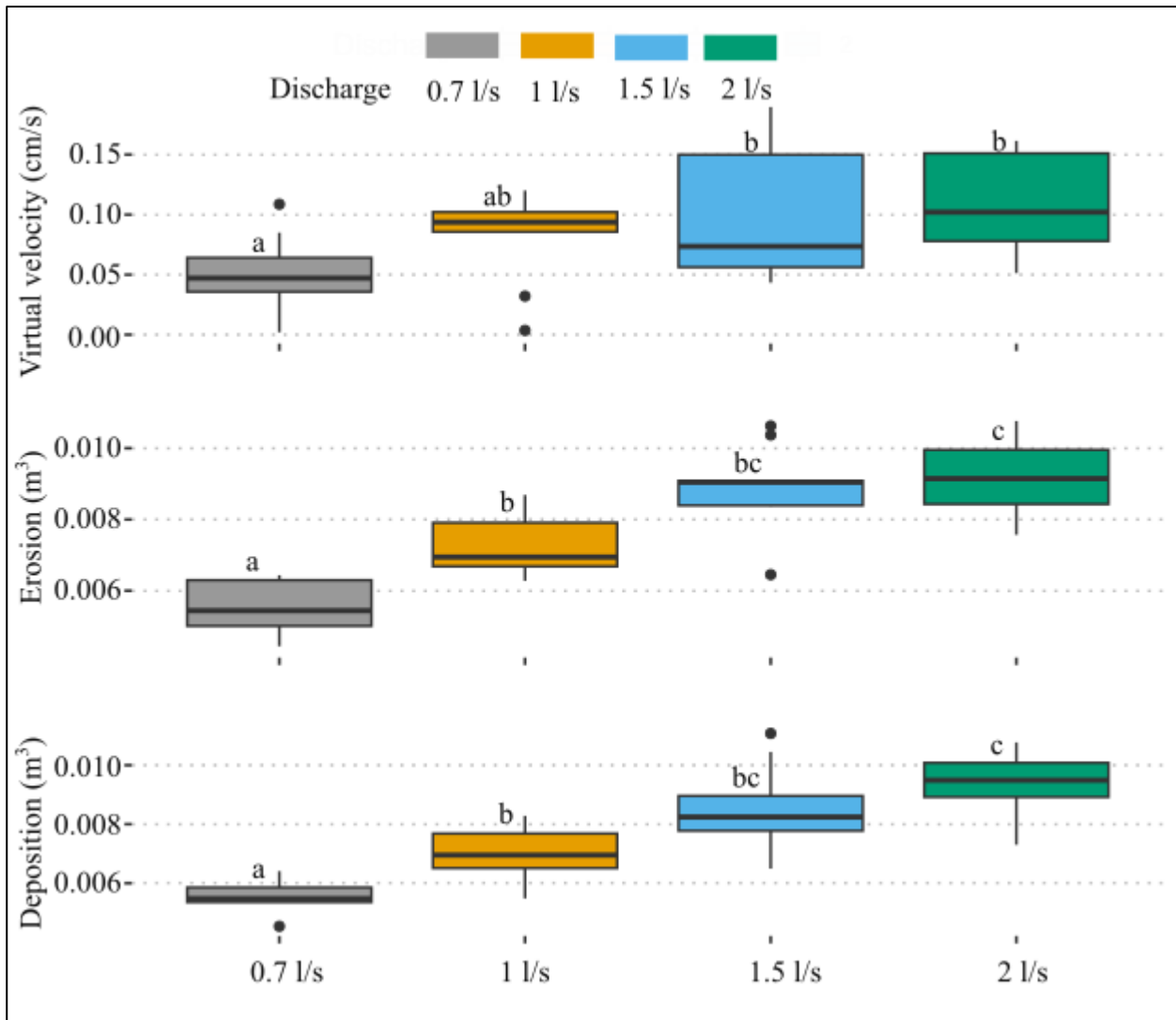
Figure 5: Estimated virtual velocity using the VMD-HD path length estimates, measured volumes of erosion and deposition for each discharge. Significant differences from the Post hoc Tukey test are denoted by letters a-c.

When used to calculate sediment transport Eq. (3) the VMD-HD method corresponds well to the measured average for the lower discharges (0.7 l/s and 1 l/s) whereas at the higher discharges (1.5 l/s and 2 l/s) the method significantly underestimated the measured flux (Fig. 6). For the 0.7 l/s discharge, the VMD-HD method estimated a rate of 0.39 g/s (SD = 0.25) averaged over the nine runs, which was not significantly different than the measured average of 0.33 g/s (SD = 0.18) and the relative percent error (δ) was 18%. For the 1 l/s discharge the method estimated 0.81 g/s (SD = 0.38) and was not significantly different than the measured average of 0.78 g/s (SD= 0.30, δ=4%). At the higher discharge of 1.5 l/s the average estimated by the VMD-HD method was 1.33 g/s (SD = 0.82) whereas the measured average was 1.98 g/s (SD = 0.70) (p-value < 0.05, δ=32%). Finally, for the 2 l/s runs the estimated average was 1.41g/s (SD = 0.48) whereas the measured average was 3.22 g/s (SD = 0.98) (p-value < 0.001, δ= 56%) (Fig. 6).

If we use just the IMF with the longest wavelength (IMF 5) to estimate path length and calculate sediment transport, we slightly overestimate sediment transport at the 0.7 l/s discharge, 0.48 g/s although not significantly (p > 0.05, δ= 45%) (Fig. 6). At the 1 l/s discharge IMF 5 significantly overestimates the average flux with an estimate of 1.03 g/s (p < 0.01, δ= 32%). At the 1.5 l/s discharge the estimated flux of 1.88 g/s using the IMF 5 path lengths was not significantly

different from the measured flux (p > 0.05, δ= 5%) (Fig. 6). However, using the IMF 5 path lengths still significantly underestimated sediment flux at the 2 l/s discharge, 1.95 g/s (p < 0.001, δ= 39%) (Fig. 6).
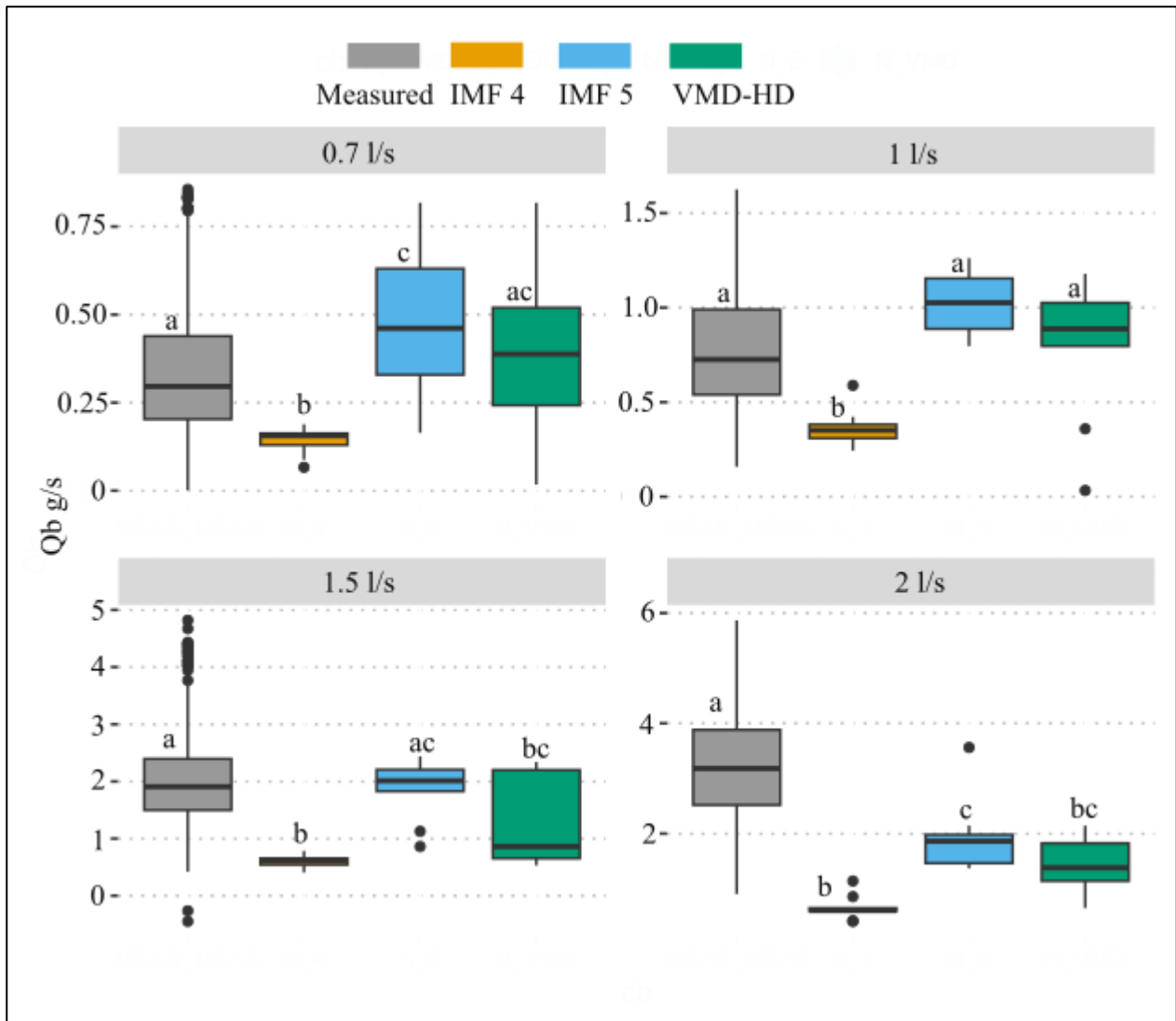
Figure 6: Measured sediment flux (gray) compared to the estimates calculated using IMF 4 (orange), IMF 5 (blue), and the VMD-HD method (green). Significant differences from the post-hoc Tukey test are denoted by letters a-c.

Using the second longest wavelength, IMF 4, we underestimate at all of the discharges (Fig. 6). The estimated flux was 0.14 g/s at the 0.7 l/s discharge (δ= 58%), 0.36 g/s at the 1 l/s discharge (δ= 54%), 0.61 g/s at the 1.5 l/s discharge (δ= 69%), and 0.65 g/s at the 2 l/s discharge (δ= 80%), (all p values < 0.001) (Fig. 6).

4.2 San Juan River

The 2018-2019 year for which we conducted our analyses, was moderate in terms of excess flow energy with 5 flood events exceeding a discharge of 500 $m^3 s^{-1}$ and a peak discharge of 942 $m^3 s^{-1}$. The path length distributions of bar 7 and bar 15 are positively skewed although there is a secondary mode in the bar 7 distribution corresponding roughly to the bar tail (Fig. 7) whereas the distribution of bar 6 is bi-modal with the primary mode corresponding to the bar apex (Fig.7). This is potentially because bar 6 had the most pronounced curvature, perhaps contributing to the clustering of deposition just before the apex, where a migrating gravel sheet terminated (McQueen et al., 2021). This bar apex corresponds with the path length from IMF 5 of 217 m which was selected from the VMD-HD method (Fig. 7). IMF 5

418   was also selected by the VMD-HD method for bar 7 equaling 324 m, and here we see a correspondence to the small

419   secondary mode where the authors note there was a clustering of tracers (Fig. 7) (McQueen et al., 2021). Again, IMF 5

420   with a path length of 323 m was also selected for bar 15 and corresponds closely to the bar apex, although there was not

421   a clustering of tracer deposition in this deployment as observed in the year with higher discharge (Fig. 7). Additionally,

422   bar 15 had the highest proportion of sand which is not represented by the tracers, potentially contributing to the

423   discrepancy between our estimates and the tracers. IMF 4 was always well below the lengths associated with the bar

424   apexes, and the median and mean tracer distances (Fig. 7). However, the bar apexes and the median and mean tracer

425   distances were always between IMF 4 and IMF 5 (Fig. 7). The range between IMF 4 and IMF 5 accounted for 62% of

426   the path length distribution for bar 6, 36% for bar 7, and 45% for bar 15.
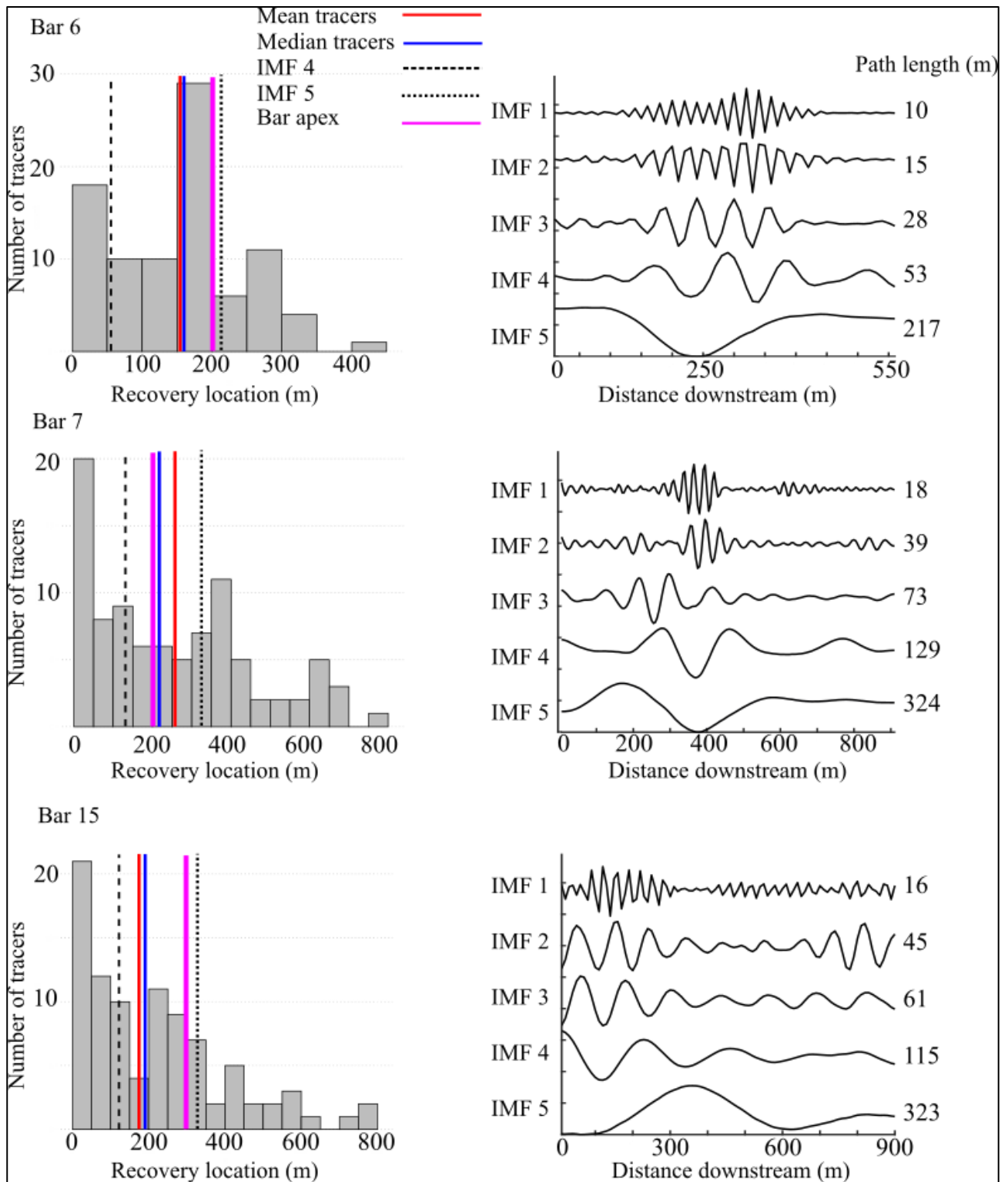
Figure 7: Tracers-based path length distributions (on the left) and VMD derived IMFs for bars 6,7, and 15 from the San Juan River dataset. IMF 4 (dashed line), IMF 5 (dotted line), mean tracer distance (red), median tracer distance (blue), and the bar apex (pink) are shown over the path length distributions.

5 Discussion

We developed a method to estimate the characteristic path length during a given flood using information inherent to the DoD by applying the principle that at channel-forming flows, the majority of particles move from an area of erosion to the next area of deposition downstream (Pyrce and Ashmore, 2003a, b). By using the periodic nature of erosion and

deposition we overcome the subjectivity and time involved in measuring these distances manually while aligning closely with these manually measured distances (Fig. 4). When evaluating the efficacy of our proposed method it is important to keep in mind the uncertainty of even direct measurement of sediment transport. The spatial and temporal frequency required to overcome the noise of measurement uncertainty (i.e., achieve an acceptable signal to noise ratio) in some cases can require sub-daily monitoring with precise equipment (Grams et al., 2019). The variability of sediment transport measurements in the flume study ranged from a standard deviation of approximately 30% to over 50% of the averaged flux (Fig. 6). Given this high variability, our reach scale averages were not significantly different from the measured averages for the 0.7 l/s and 1 l/s discharges (Fig. 6). Importantly, we observed that the method underestimates the sediment flux significantly for the two highest discharges in the lab where the bed shows a higher percentage of the width experiencing topographic change (Fig. 6). The method presented to estimate a characteristic path length using only remotely sensed data shows promising results under certain conditions and provides insight into conditions where it is not applicable.

5.1 Path length estimation by VMD-HD method: limitations and perspectives

5.1.1 Flow effects

Previous studies have shown a relationship between path length and hydrologic variables such as discharge, stream power, and excess shear stress (Hassan et al., 1991; Pyrce and Ashmore, 2003b). A notable result of the flume experiment is that the estimated path length did not significantly differ between the four discharges (Fig. 5). We propose two possible explanations for this discrepancy with the literature. First, it is possible that the actual path length is increasing with discharge as has been observed in previous studies (Hassan et al., 1991; Pyrce and Ashmore, 2003b) but the method fails to capture it because the VMD-HD method is based on the spacing of erosion and deposition which does not change for the varying discharges under the flume conditions. It is possible that at higher discharges the characteristic path length, that we define as the distance from net erosional areas to net depositional areas, is not appropriate under the higher flow conditions because most particles are moving farther than the next depositional site downstream. This violates the assumption on which our method is based and is impossible to prove in our experiment without tracers. We can however look to literature to understand the conditions in which tracers tend to travel more than one morphological unit (Liébault et al., 2012; Vázquez-Tarrío et al., 2019) and coupled with future studies, perhaps determine the conditions under which a characteristic path length is inappropriate to estimate sediment transport.

From the San Juan River data we see that for a year with moderate flow, as characterized by the authors, that very few tracers traveled further than the first depositional site downstream of their insertion point although it is possible that the unrecovered tracers escaped the first bar, the recovery rates were high with 75% of tracers recovered for bars 6 and 15, and 79% recovered for bar 7 (McQueen et al., 2021). However, the moderate flow year for which we had corresponding tracer and DoD data resulted in two of the three sites with positively skewed distributions, and only bar six showing a mode near the bar apex, which also corresponded to the IMF 5 path length (Fig. 7). The moderate flow conditions could explain why our estimates lined up more closely with the bar apex for bar 15, where in the previous high flow year the majority of tracers were deposited resulting in a symmetrical distribution (Fig. 8 from McQueen et al., 2021). It could be that our method is strongly influenced by the morphology of the channel such that when flow is insufficient to create symmetrical or bi modal path length distributions, we overestimate by using the characteristic path length because the majority of particles are not reaching the next major depositional site downstream (i.e., a positively skewed distribution). Additionally, when the flow exceeds a yet unidentified threshold, the majority of particles move more than one depositional site downstream and therefore we underestimate sediment transport by using the characteristic path

length. We can speculate that this is happening to some extent in the flume experiment. We see that at the lowest discharge, 0.7 l/s, we slightly overestimate the sediment flux especially using IMF 5 (Fig. 6) and underestimate the flux at the highest discharge, 2 l/s, where we also see a simplification of channel morphology (Fig. 6, 3). Because we did not have tracers in the flumes we can not say if the path length distributions were in fact different between the lowest and highest discharges. Future applications of this method with tracer data both in the flumes and in the field could help to understand when the characteristic length scale of morphology extracted by the method is an appropriate estimate of sediment transport and if this corresponds to flow metrics and path length distributions. In the flume studies we tested the idea that the majority of particles are bypassing the first depositional site simply by doubling the estimated path length. Assuming that sediment is not trapped in the first depositional area but in the second one and doubling the path length we more closely estimate the sediment transport at the higher discharges (i.e., estimates are not significantly different than the measured averages ($p>0.05$) but overestimate the sediment transport at the 0.7 l/s and 1 l/s discharges ($p<0.05$) (Fig. A5).

5.1.2 Confinement

It is possible that due to the confined condition of the flumes, channel width may exert an outsized effect on the average bedload transport distance as the channel is unable to widen in response to an increase in discharge, therefore causing a flushing effect. In the flume experiment, we found that the VMD-HD method performed better at the lower discharges of 0.7 l/s and 1 l/s but significantly underestimated the sediment transport at the 1.5 l/s and 2 l/s discharges (Fig. 6). The underestimation at higher discharges could be related to the amount of morphological change relative to the sediment transport. Recently, Booker and Eaton (2022) quantitatively explored the link between sediment transport and morphology and proposed an index to represent the intuitive notion that as sediment transport increases relative to morphological change, the processes become decoupled and inferences from one to another become more difficult. They developed a 'throughput index' which is the ratio between sediment flux and morphological change and represents how much sediment moves through a reach without leaving a topographic signature of equal magnitude. Therefore, the ratio represents how well the flux is represented morphologically with the ratio approaching 1 when all of the flux is shown as morphological change and exceeding 1 when there is transport without equivalent morphological change. In our case the flume experiments were confined, therefore, as discharge increased the channel was not able to widen and deform laterally potentially causing the sediment to move through the flume without leaving an equivalent topographic signature. To explore the applicability of the method proposed we calculated the morphological active width by counting the percentage of pixels in the DoD that showed topographic change after filtering (we applied this metric only for the flume experiments since the San Juan River DoDs do not include the submerged part of the channel). The morphological active width increased with discharge as expected and was positively correlated with the error of our estimates (Fig. 8). This result exposes a limitation of the morphological method in general and our application specifically, that is, confined channels with high transport relative to morphological change are likely poor candidates for the morphological method as inferences between changes in morphology and sediment transport become decoupled. Further applications of this method in the field and in the lab could identify a potential threshold defined by the throughput index (Booker and Eaton, 2022) or the morphological active width described in this study. The advantage of using the morphological active width as opposed to the throughput index is that it can be determined from the DoD without direct sediment transport measurements.

513
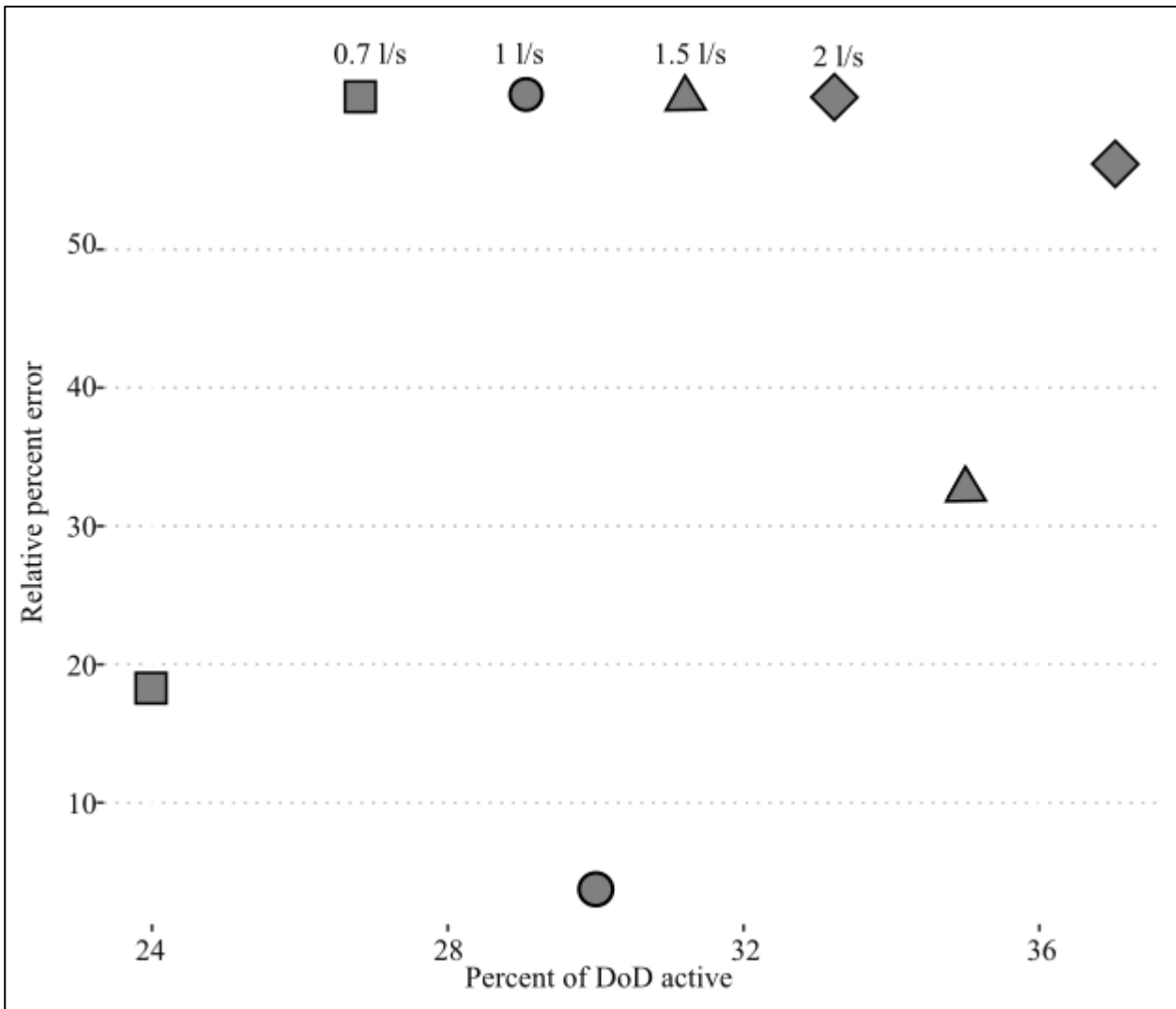
Figure 8: Relative percent error between estimated flux using the VMD-HD method and the measured flux in the
flume experiments (y-axis) vs the percentage of the DoD showing morphological change (x-axis). Different
discharges are denoted by shape.

5.1.3 Morphological controls

Previous studies have shown that in gravel bed rivers, macroform spacing is typically 5-7 channel widths (Montgomery

and Buffington, 1997) and therefore half of that spacing, i.e. pool to bar, may be considered a proxy for the

characteristic path length. We compared our estimates of path length to (half) of both 5 and 7 times the channel width in

the flumes and found that the IMF 5 estimates of path length were between the 5 and 7 channel widths for all but the

highest discharge (Fig. A6). Interestingly, the manually measured distances were less than the 5-7 channel widths for all

discharges but approaching 5 channel widths at the 2 l/s discharge (Fig. A6). When used to calculate sediment flux, the

estimates derived from using 5 and 7 channel widths were not significantly different than our VMD-HD estimates at

discharges 0.7-1.5 l/s or the measured flux at all discharges (Fig. A5). Here we are likely seeing a good correspondence

between the characteristic path length, width, and sediment transport, because at formative discharges, morphology is

the primary control on bedload travel distance. Whereas at lower discharges, where the morphology is relatively stable,

discharge may exert a stronger control on path length. Because we do not have tracer data in the flumes for comparison,

we can only rely on the sediment transport measurements for validation but further flume studies with both sediment

flux and tracer data for validation could help resolve this question. The periodicity we extract from the DoDs as an

531 estimate of path length corresponds to previous observations of preferential particle deposition at specific

532 morphological units and relationships to channel morphology (Beechie, 2001; Pyrce and Ashmore, 2003a, b; Kasprak et

533 al., 2015; McDowell and Hassan, 2020; McDowell et al., 2021). In the San Juan River study, our estimates aligned

534 closely with the secondary modes in the particle path length distributions (Fig. 7) consistent with observations that at

535 channel forming flows, particle path lengths tend to be bi or multimodal with secondary modes corresponding to the

536 location of bars (Pyrce and Ashmore, 2003b). This preliminary result should be further examined with additional field

537 data in multi-threaded channel types.

538 We expected that the path length in more complex channels such as braided configurations would be more difficult to

539 estimate due to the possibility of multiple path lengths active at different flow stages. In this study both the flume

540 experiment and the field study exhibited a wandering morphology although in the flume experiment, the channel began

541 to simplify at higher discharges, likely due to the inability of the channel to widen in response to the increase in

542 discharge. Further, path length estimates did not change significantly between the discharges whereas the erosion

543 volume increases with discharge, and that, as mentioned previously, potentially contributed to the underestimation of

544 sediment flux at the higher discharges. Additionally, at the 1.5 l/s, and 2 l/s discharges, the patches of erosion and

545 deposition began to overlap, therefore, the wavelike pattern from areas of erosion to deposition represented by the IMF

546 5 vector became flattened (Fig. 3, A1). To disentangle the confounding erosion and deposition from the net vector, we

547 applied the VMD method to a vector created from erosion and deposition separately. When calculating the path length

548 using the erosion or deposition vectors, we took half of the resulting path length as we are still interested in the distance

549 from erosion to deposition rather than erosion to erosion. We found that the path lengths generated from these vectors

550 were not significantly different than the path lengths generated using the net vector ($p > 0.05$) (Fig. A6) nor were the

551 estimates of sediment transport (Fig. A5) This evidence supports the use of the net vector in this case because it appears

552 that erosion and deposition were similarly distributed. However, in rivers with differing morphology, perhaps braided

553 systems, we might suspect that erosion will be more localized than deposition which can be dispersed (Goff and

554 Ashmore, 1994). In these cases, using VMD to decompose the net, erosion, and deposition separately could give further

555 insight into how deposition and erosion are contributing to the net change. For example, deposition may contribute little

556 to net vector if the relative magnitude of the oscillations is small compared to erosion which tends to be more

557 concentrated. In addition to estimating a characteristic path length, this decomposition could give further insight into the

558 nature of depositional and erosional processes in a reach. We also recognize that perhaps when multiple channels are

559 present and active, it may be beneficial to segregate the DoD, treating each channel as a separate system and generate

560 multiple path length estimations and avoid compensating erosion and deposition within the cross section. Further

561 investigations are needed in the lab and in the field to propose robust methodologies to assess realistic ranges of path

562 lengths from DoD for varying river patterns.

563 **5.1.4 Using the IMFs**

564 The path length-based method for calculating sediment transport necessitates that a single path length be selected and

565 this is surely an oversimplification of reality. Encouragingly, the flume experiment shows that by using the VMD-HD

566 method to select the path length, we are able to reasonably approximate sediment transport at the lower discharges (Fig.

567 6). However, when applying this method to a real case study, like that of the San Juan River, it is important to consider

568 if the results make sense given what is known about the channel and the time and magnitude of flood events between

569 surveys, potentially taking into account both IMF 4 and IMF 5 to generate a range of plausible transport or path lengths.

570 The VMD-HD method presented here selects one of the five IMFs to be used as an estimate of path length based on the

geometric similarity, as measured by the Hausdorff distance, of the IMF to the original data vector. However, we presume that not only does the method occasionally select an erroneous IMF (IMF 1 for example where the path length is on the order of mm) but it also reasons that in some cases more than one IMF could represent the pattern of erosion and deposition in the DoD or perhaps a range due to the heterogeneous nature of sediment transport. In the flume experiment, the VMD-HD method selected the longest wavelength, IMF 5, 74% of the time and IMF 4, 24% of the time. There were only two instances in which IMF 1 was selected and neither IMF 2 or 3 were ever selected. Likewise, IMF 5 was selected for all three bars in the San Juan River dataset. This result agrees with observations from the signal processing literature wherein the lower frequency (in our case wavelength) IMFs (4 and 5) are thought to represent the true signal whereas the higher frequency (shorter wavelength) IMFs are attributed to noise (Boudraa et al., 2005). In our case we can verify visually that IMF 5 is most likely representative of the characteristic path length by tracing the path from erosional site to depositional site within the DoD using the manual method (Fig. 9). Here we see that the longest IMF captures the spacing between erosional and depositional patches as estimated by other methods (Redolfi, 2014; Vericat et al., 2017; Calle et al., 2020). This study, as the others, supports the idea that the periodic nature of erosion and deposition can be used to estimate sediment transport and helps to clarify the conditions where this approach is valid. Moreover, this study provides an objective and repeatable method to estimate the characteristic path length.
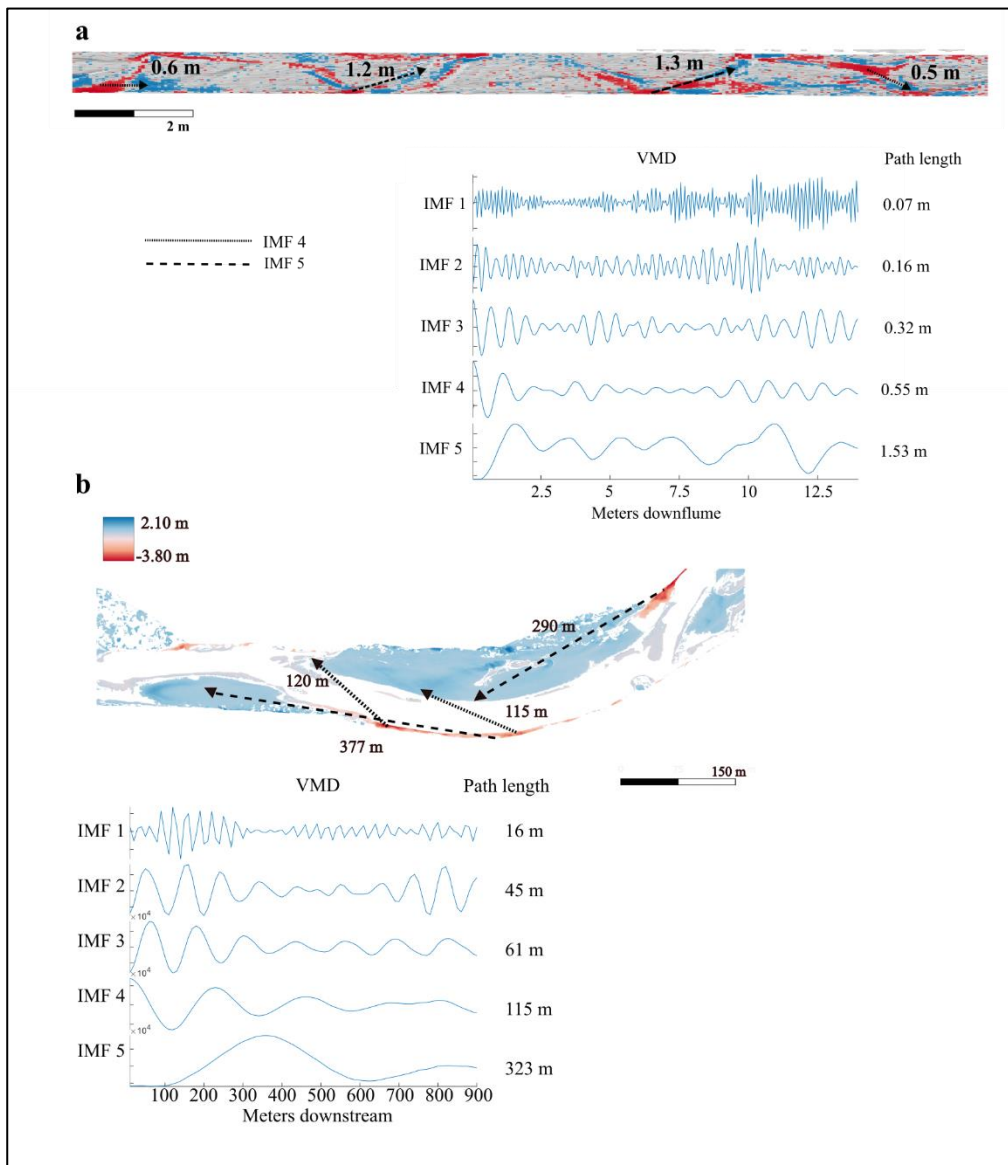
Figure 9: DoD with arrows showing possible path lengths between areas of erosion (red) to deposition (blue) corresponding to both IMF 4 and IMF 5. The VMD breakdown including all IMFs and the corresponding path lengths are shown for an experimental run from the 1.5 l discharge (a) and bar 15 from the San Juan River (b).

Different IMFs also allow us to explore multiple periodicities, such as shorter path lengths in the DoDs that may correspond to IMF 4 (Fig. 9). The method we present here to select one of the IMFs to represent the periodicity is convenient for assigning a characteristic path length to be used in sediment transport calculations. However, it is unclear if the range of IMFs may be used to estimate aspects of the path length distribution. As a first step, we see that in the San Juan River the path lengths associated with IMF 4 and IMF 5 bracket the mean, median, and key depositional areas associated with the path length distribution (Fig. 7). With future studies it may be possible to set a range of plausible transport based on IMFs 4 and 5.

5.2 DoD related uncertainties

Any application of the morphological method using DoDs is sensitive to the error thresholding method used due to the way in which different thresholding techniques influence both the volumes of erosion and deposition as well as their spatial patterning (Brasington et al., 2003; Wheaton, 2008; Wheaton et al., 2010; Vericat et al., 2017). Because our method relies on the spacing between areas of erosion and deposition which is related to the size of the patches as well as which patches are detected, we considered that thresholding techniques could greatly affect the estimates of path length. We tested this hypothesis by applying the method to both the raw and filtered DoDs for the Trento flume experiment and found that while the volumes of erosion and deposition were lower after thresholding as expected ($p < 0.001$), the path length estimates were not significantly different ($p > 0.05$) (Table A1). While the thresholding here did not affect the path length estimates, we might imagine a scenario in which an entire area of erosion or deposition is removed through aggressive thresholding techniques, thereby potentially affecting the path length estimates and therefore caution that appropriate thresholding is important for the application of this method and the morphological method in general. It is also important to consider the spatial resolution (i.e. raster cell size) of the DoD when applying this method. Similarly to thresholding or selecting a bin size, the spatial resolution of the DoD could cause information to be lost if the cell size is large enough to aggregate erosion and deposition within the same cell (see for instance the comparison made in Antoniazza et al., 2019). We see less of a risk in using smaller cell sizes as the method already calls for aggregation in the binning process and in theory VMD should be able to separate the small scale fluctuations as short wavelength IMFs. However, this is an open question and should be evaluated by the user on a case by case basis.

The time between surveys is of equal importance to the path length in the estimation of virtual velocity and in the field can be highly uncertain due to poor availability of hydrologic data and/or the uncertainty of estimating the onset of transport based on a critical shear stress. Further, as time between surveys increases, so too does the probability of compensating erosion and deposition which can affect both the volumes of erosion and deposition and the topographic signatures (Lindsay and Ashmore, 2002; Vericat et al., 2017) necessary for VMD-HD method. We tested how the time between surveys might affect both the volumes of erosion and deposition and our path length estimates by differencing DEMs not every time step but between two, three, and four timesteps, each time step being one of the nine runs in the lab of phase 3 (see method). Not surprisingly the volume of erosion and deposition increased significantly with increasing time between surveys with the largest increase between the 1st timestep and 2nd timestep (Fig. 10). The path length estimates did not increase significantly for any of the discharges (Fig. 10c) indicating that the path length estimate is stable, likely because, as already noted, the spacing of erosion and deposition is related to the position of erosional and depositional features which do not change much in the flume. When both of these parameters are used in the sediment transport calculations and normalized by the increased time between surveys, we found no statistically

628 significant difference between the estimates (Fig. 10d). However, though not statistically significant, there is an

629 apparent decreasing trend in the sediment flux with the increased time between surveys, especially for the 2 l/s

630 discharge that may indicate compensation (Fig. 10d). Despite the apparent trend at the highest discharge this is a

631 promising result in that even by increasing the time interval by a factor of 4 we are still able to estimate sediment

632 transport reasonably at the lower discharges. In the field there are often multiple flood events of differing magnitude in

633 the year between surveys as was the case with the San Juan River study (McQueen et al., 2021). Although there were

634 five flood events of differing magnitudes between the San Juan River surveys, we were still able to estimate path

635 lengths corresponding to potentially significant features of the path length distributions (Fig. 7).

636
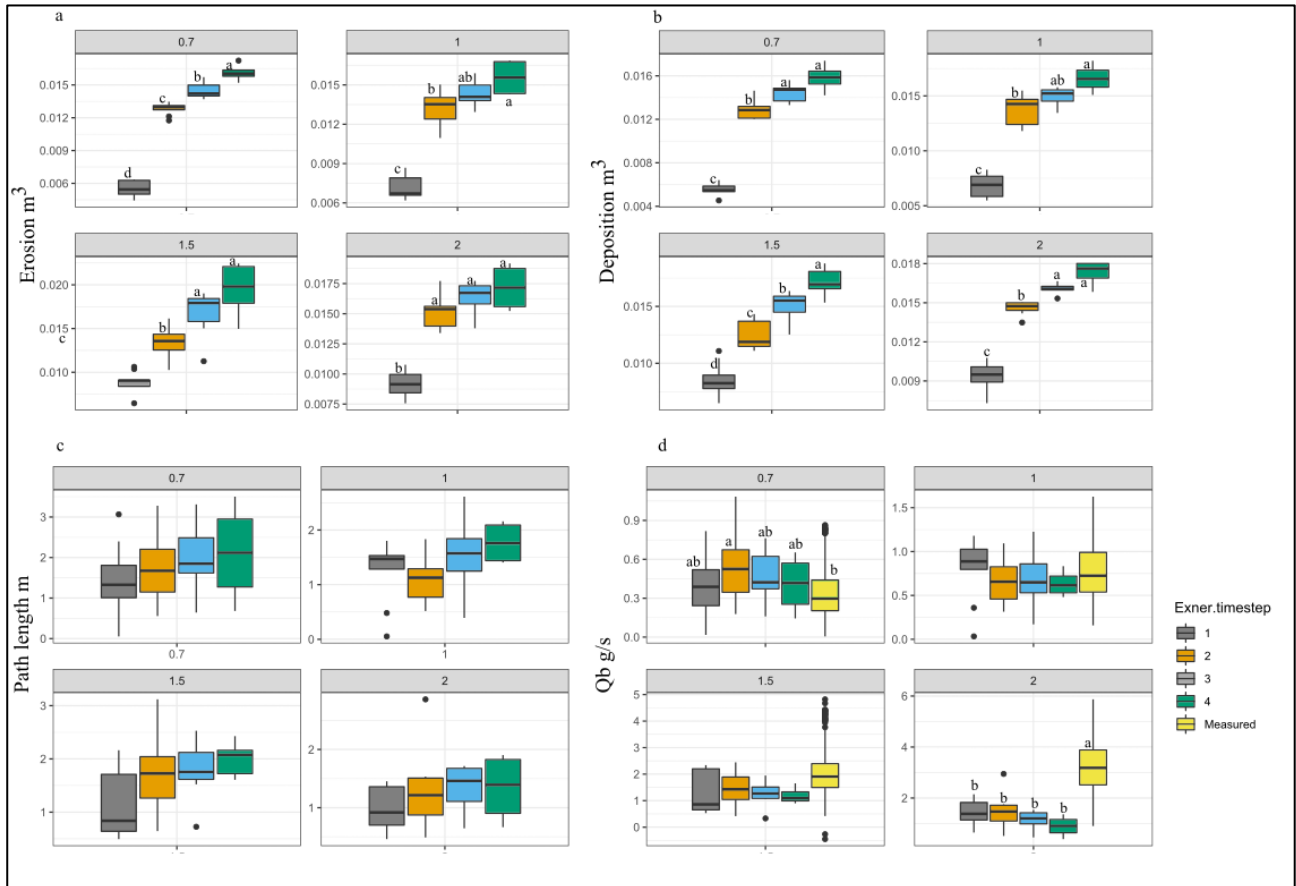
Figure 10: (a) Erosion measured from the flume experiments for each discharge and each timestep (b) deposition (c) path length estimates using VMD-HD method (d) sediment flux estimated using VMD-HD method and measured. Significant post-hoc Tukey results are denoted by letters a-d (α=0.05).

6 Conclusion

641 Given the observed connections between morphology and path length at channel forming flows, we proposed that the

642 periodic nature of the pattern of erosion and deposition can be a proxy for a characteristic path length in gravel bed

643 rivers. We applied tools from signal processing to quantify this periodicity and found that by the longest wavelengths

644 from the decomposition, IMF 4 and IMF 5 may represent meaningful bedload transport processes and IMF 5 in

645 particular may represent the characteristic path length. We found that the path length estimates generated by IMFs 4 and

646 5 bracket a significant portion of measured path length distributions in the field and correspond to important

647 morphological units. In the flume experiment we found that IMF 4 and 5 path lengths also bracket the manually

648 measured distances between erosional and depositional patches and when extended to calculate sediment flux our

649 estimates were not significantly different from the measured average at low discharges. Importantly we found an

650   insensitivity of the method to increasing discharge and propose that perhaps limits arise where discharge increases in

651   confined settings, such as in the flume, and sediment transport becomes decoupled from morphological changes. Our

652   method provides a new view of the periodic nature of erosion and deposition in sediment transport and a novel way to

653   extract sediment transport information using only DoDs.

654

655

656   **Appendix A**

657
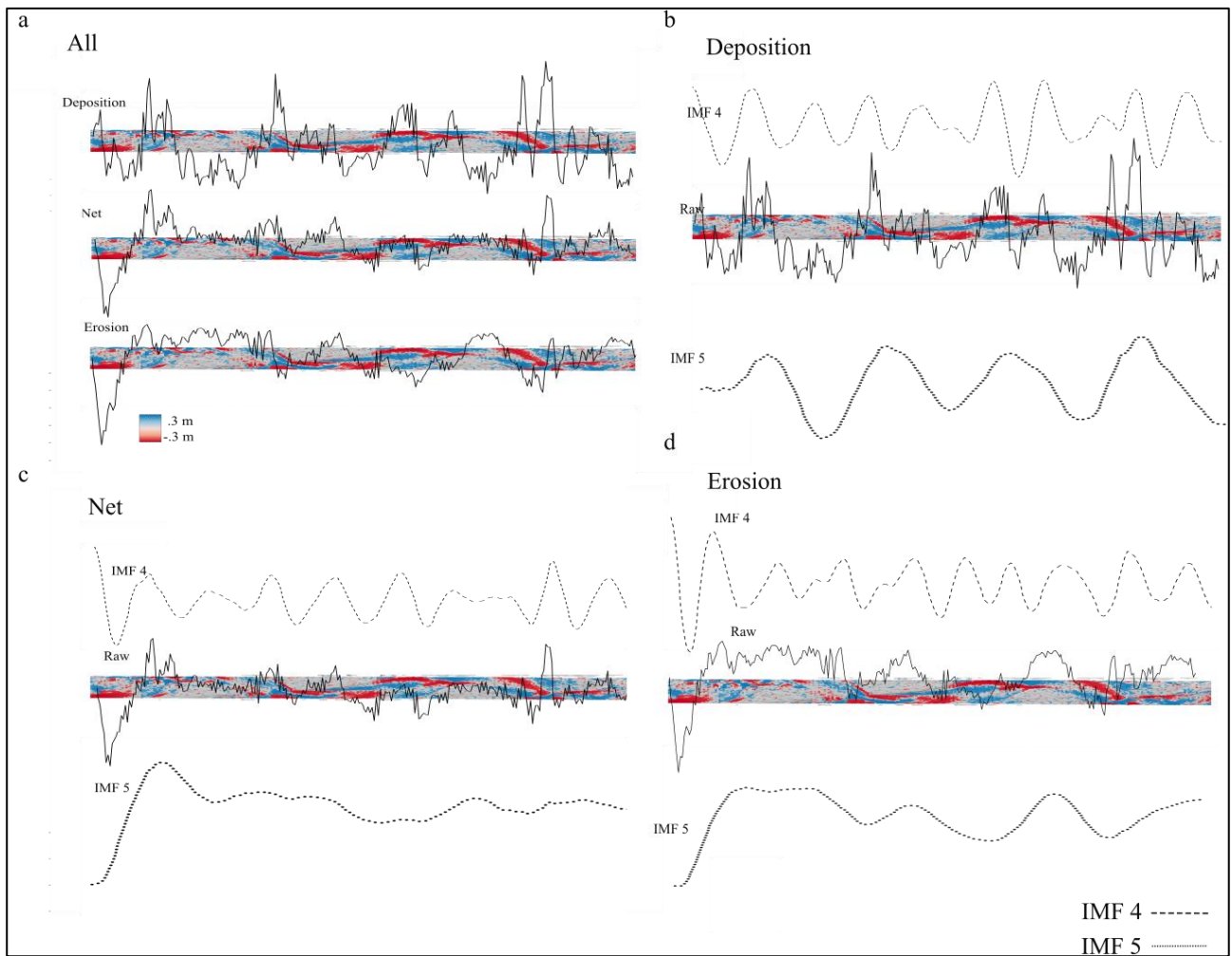
659   Figure A1. DoDs from the 2 l/s discharge. a) Vector of deposition, erosion, and the net. b) Raw depositional vector and
660   the decomposition of IMF 4 and IMF 5 from that depositional vector. c) Net vector and the decomposition of IMF 4 and
661   IMF 5 from that net vector. d) Raw erosional vector and the decomposition of IMF 4 and IMF 5 from that erosional
662   vector.

663
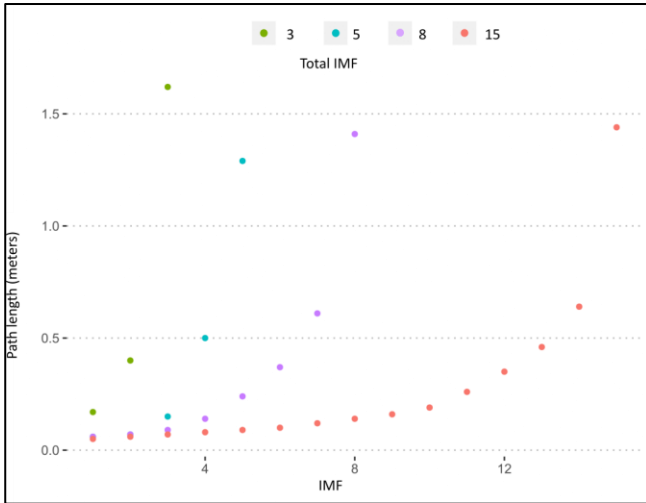
664

665 Figure A2. Path length estimates using a maximum of 3,5,8, or 15 IMFs.
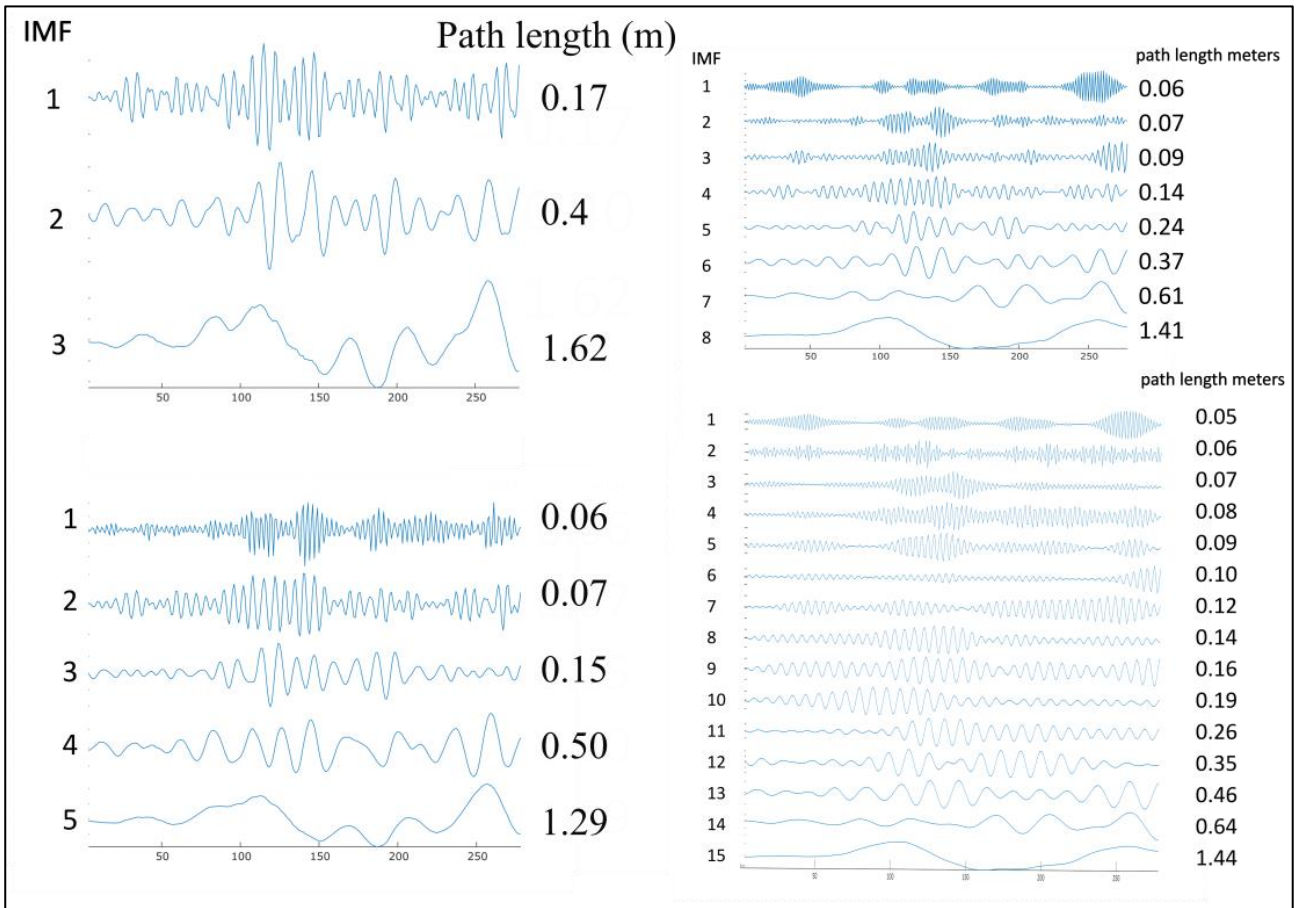
666

667 Figure A3. Path length estimates from VMD for 1.5 l/s discharge. Sensitivity of maximum number of IMFs.

668
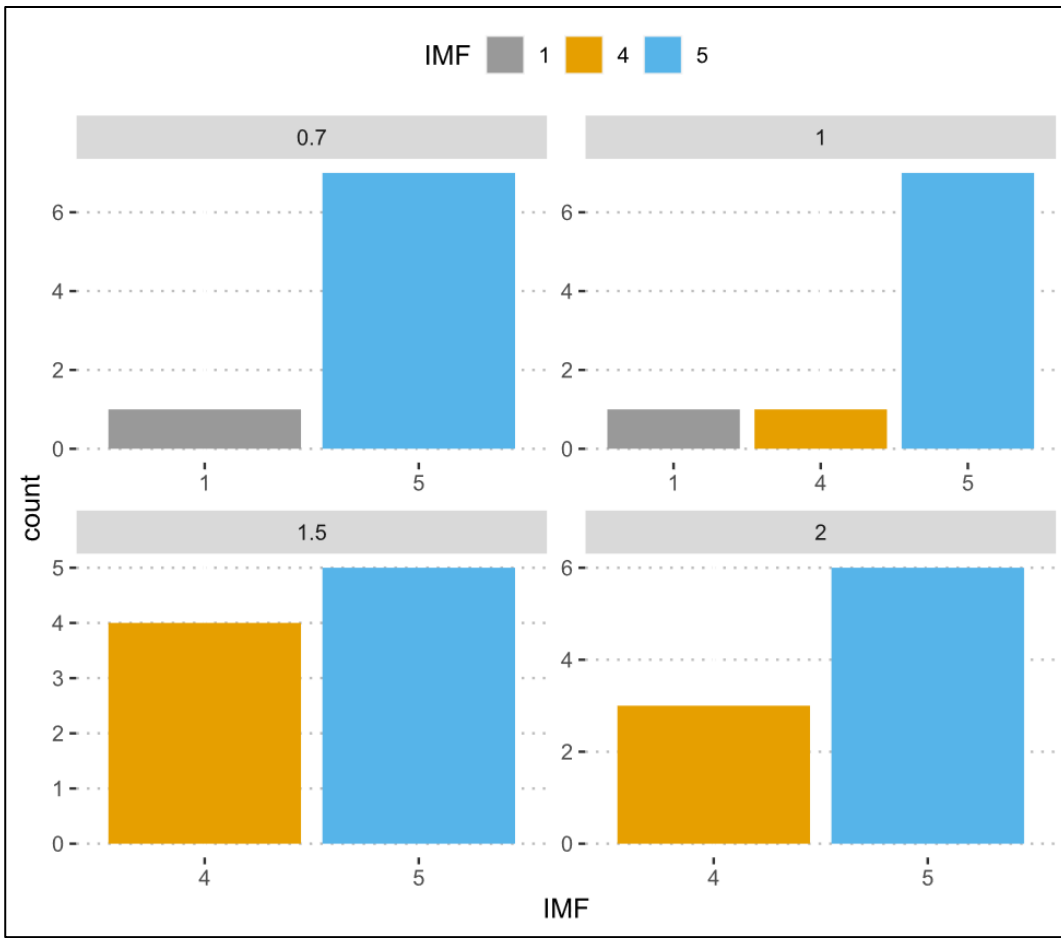
669

670   Figure A4. Number of times each IMF was selected by the VMD-HD method for each discharge.
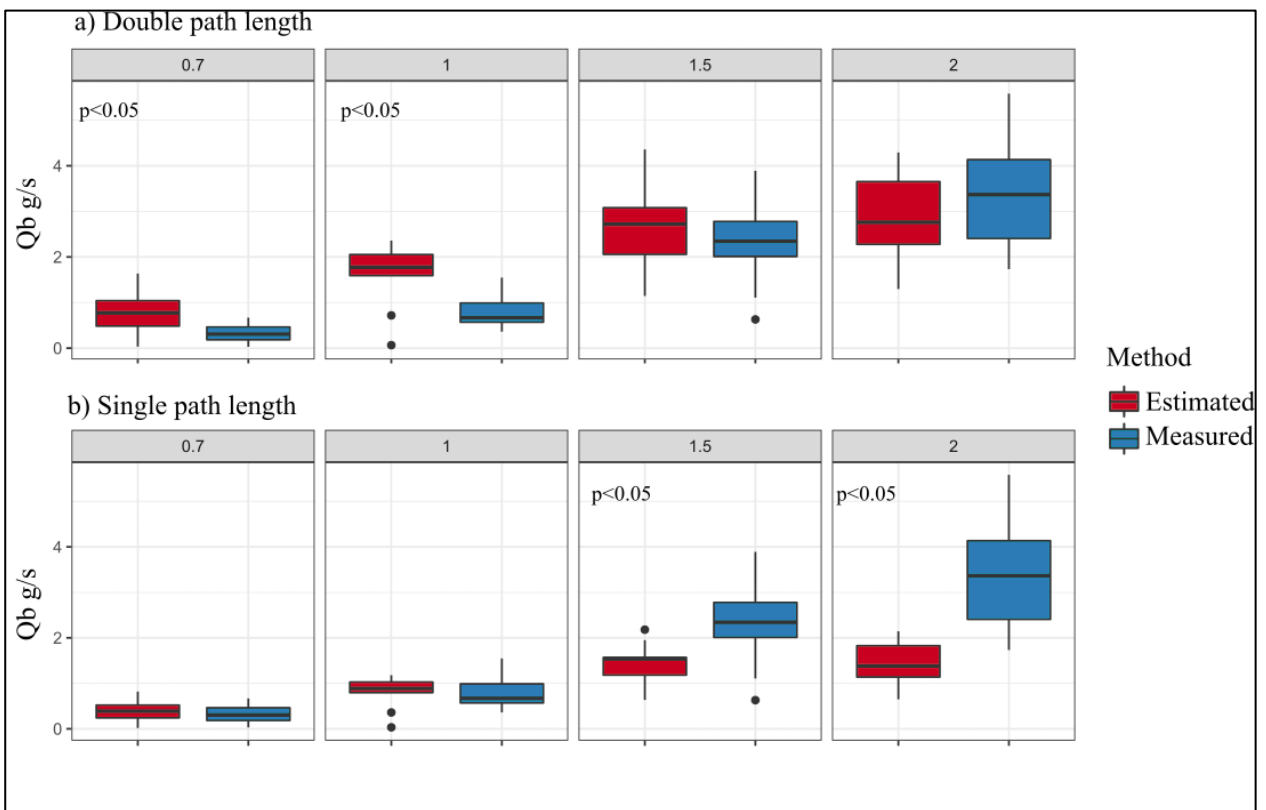
671

672 Figure A5. Sediment transport calculated using the single path length estimate from the VMD-HD method (b) and
673 doubling the path length estimate (a). Estimated flux is red and measured flux is blue. Significant p values are shown.

674
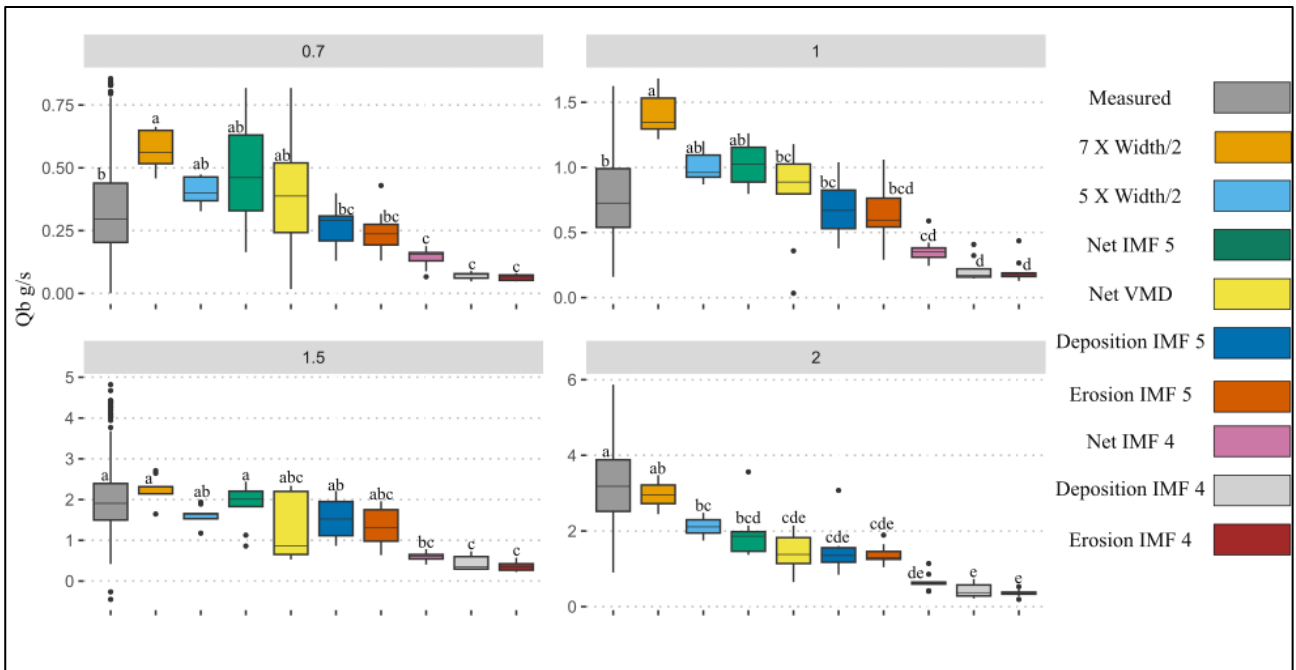
675

676 Figure A6. Sediment transport (g/s) calculated using channel dimensions, IMFs 4 and 5 for net, erosion, and deposition
677 vectors. Compared to the measured flux for each discharge. Post hoc Tukey results denoted by letters a-f.
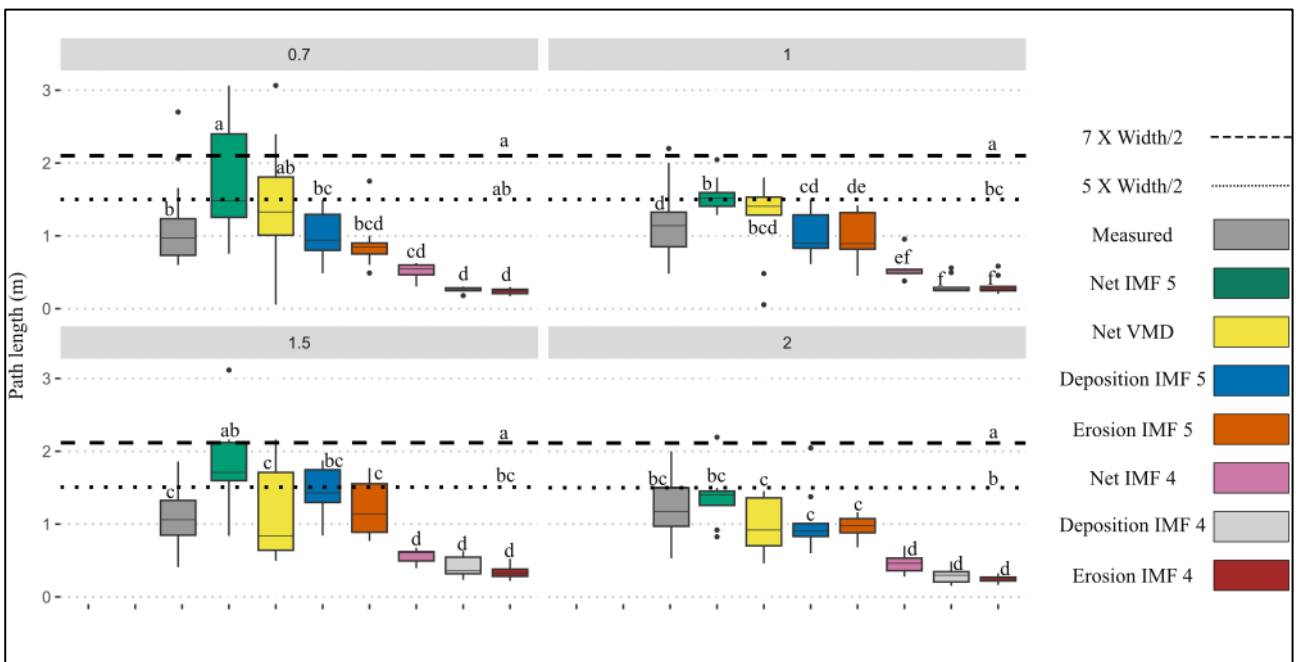
678

679 Figure A7. Path length estimates from the channel dimensions, IMFs 4 and 5 for net, erosion, and deposition vectors
680 compared to manually measured distances for each discharge. Post hoc Tukey results denoted by letters a-f.

681 Table A1. Results from filtered vs raw DoDs from the flume experiments.

Discharge	Path length raw (m)	Path length filtered (m)	Qb estimated raw(g/s)	Qb estimated filtered (g/s)	Erosion raw (m3)	Deposition raw(m3)	Erosion filtered (m3)	Deposition filtered (m3)

0.7	1.77	1.31	0.69	0.30	0.01	0.01	0.01	0.01
0.7	0.80	0.75	0.29	0.14	0.01	0.01	0.00	0.00
0.7	3.05	3.06	1.20	0.71	0.01	0.01	0.01	0.01
0.7	2.54	2.40	0.97	0.51	0.01	0.01	0.01	0.01
0.7	2.30	0.05	1.01	0.01	0.01	0.01	0.01	0.01
0.7	0.87	1.09	0.35	0.23	0.01	0.01	0.01	0.01
0.7	1.57	1.61	0.70	0.43	0.01	0.01	0.01	0.01
0.7	1.24	1.35	0.56	0.37	0.01	0.01	0.01	0.01
1	1.25	1.41	1.04	0.89	0.01	0.01	0.01	0.01
1	1.37	0.48	1.28	0.31	0.01	0.01	0.01	0.01
1	1.25	1.47	1.10	1.02	0.01	0.01	0.01	0.01
1	1.23	1.80	1.18	1.00	0.01	0.01	0.01	0.01
1	1.48	1.59	1.46	0.84	0.01	0.01	0.01	0.01
1	1.83	1.53	1.57	0.77	0.01	0.01	0.01	0.01
1	1.54	1.52	1.27	0.75	0.01	0.01	0.01	0.01
1	1.51	1.29	1.21	0.69	0.01	0.01	0.01	0.01
1.5	1.12	0.68	1.82	0.53	0.01	0.01	0.01	0.01
1.5	1.63	0.84	2.30	0.86	0.01	0.01	0.01	0.01
1.5	1.50	0.64	2.74	0.65	0.02	0.01	0.01	0.01
1.5	0.50	0.61	0.82	0.67	0.01	0.01	0.01	0.01
1.5	0.85	0.49	1.41	0.54	0.01	0.01	0.01	0.01
1.5	0.51	1.60	0.76	2.01	0.01	0.01	0.01	0.01
1.5	1.67	1.71	2.28	2.21	0.01	0.01	0.01	0.01
1.5	1.50	2.16	2.54	2.20	0.01	0.01	0.01	0.01
1.5	1.13	2.12	1.73	2.34	0.01	0.01	0.01	0.01
2	1.41	1.40	2.53	1.86	0.01	0.01	0.01	0.01
2	0.91	0.92	1.58	1.19	0.01	0.01	0.01	0.01
2	1.26	1.36	2.05	1.58	0.01	0.01	0.01	0.01
2	1.13	1.26	1.67	1.27	0.01	0.01	0.01	0.01
2	0.06	1.45	0.09	1.61	0.01	0.01	0.01	0.01
2	0.46	0.46	0.78	0.56	0.01	0.01	0.01	0.01
2	1.32	0.83	2.04	1.18	0.01	0.01	0.01	0.01
2	0.71	0.66	1.30	0.74	0.01	0.01	0.01	0.01
Summary								
Discharge	Erosion	Deposition	Path Length	Qb				
0.7	$p<0.001$**	$p<0.001$**	$p>0.05$	$p<0.05$*				
1	$p<0.001$**	$p<0.001$**	$p>0.05$	$p<0.05$*				
1.5	$p<0.001$**	$p<0.001$**	$p>0.05$	$p<0.05$*				
2	$p<0.001$**	$p<0.001$**	$p>0.05$	$p>0.05$				
*p-values from student's t test between raw and filtered data								

682

Data availability
Data is available at https://doi.org/10.5281/zenodo.8014453.

Author contribution

LC, SB, WB and NS conceptualized the study. EP preformed the experiments. LC, SB and WB designed the method. LC performed statistical analysis. LC, EP, and WB wrote the manuscript. LC, SB, EP, WB, and NS edited the manuscript.

Competing interests

The authors declare they have no competing interests.

Financial support

This work was supported by the CARIPARO foundation and the University of Padova.

References

Antoniazza, G., Bakker, M., and Lane, S. N.: Revisiting the morphological method in two-dimensions to quantify bed-material transport in braided rivers, Earth Surf. Process. Landf., 44, 2251–2267, https://doi.org/10.1002/esp.4633, 2019.

Ashmore, P. E. and Church, M.: Sediment transport and river morphology: a paradigm for study, Gravel-Bed Rivers Environ., 345, 115–139, 1998.

Bakker, M., Antoniazza, G., Odermatt, E., and Lane, S. N.: Morphological Response of an Alpine Braided Reach to Sediment-Laden Flow Events, J. Geophys. Res. Earth Surf., 124, 1310–1328, https://doi.org/10.1029/2018JF004811, 2019.

Barnhart, B. L. and Eichinger, W. E.: Empirical Mode Decomposition applied to solar irradiance, global temperature, sunspot number, and CO2 concentration data, J. Atmospheric Sol.-Terr. Phys., 73, 1771–1779, https://doi.org/10.1016/j.jastp.2011.04.012, 2011.

Beechie, T. J.: Empirical predictors of annual bed load travel distance, and implications for salmonid habitat restoration and protection, Earth Surf. Process. Landf., 26, 1025–1034, https://doi.org/10.1002/esp.251, 2001.

Booker, W. H. and Eaton, B. C.: Morphodynamic styles: characterising the behaviour of gravel-bed rivers using a novel, quantitative index, Earth Surf. Dyn., 10, 247–260, https://doi.org/10.5194/esurf-10-247-2022, 2022.

Boudraa, A.-O., Cexus, J.-C., and Saidi, Z.: EMD-Based Signal Noise Reduction, Signal Process., 1, 2005.

Brasington, J., Rumsby, B. T., and McVey, R. A.: Monitoring and modelling morphological change in a braided gravel-bed river using high resolution GPS-based survey, Earth Surf. Process. Landf., 25, 973–990, https://doi.org/10.1002/1096-9837(200008)25:9<973::AID-ESP111>3.0.CO;2-Y, 2000.

Brasington, J., Langham, J., and Rumsby, B.: Methodological sensitivity of morphometric estimates of coarse fluvial sediment transport, Geomorphology, 53, 299–316, https://doi.org/10.1016/S0169-555X(02)00320-3, 2003.

Brenna, A. and Surian, N.: Coarse sediment mobility and fluxes in wide mountain streams: Insights using the virtual velocity approach, Geomorphology, 427, 108625, https://doi.org/10.1016/j.geomorph.2023.108625, 2023.

Brenna, A., Surian, N., and Mao, L.: Virtual Velocity Approach for Estimating Bed Material Transport in Gravel-Bed Rivers: Key Factors and Significance, Water Resour. Res., 55, 1651–1674, https://doi.org/10.1029/2018WR023556, 2019.

Brenna, A., Surian, N., Ghinassi, M., and Marchi, L.: Sediment–water flows in mountain streams: Recognition and classification based on field evidence, Geomorphology, 371, 107413, https://doi.org/10.1016/j.geomorph.2020.107413, 2020.

Brewer, P. A. and Passmore, D. G.: Sediment budgeting techniques in gravel-bed rivers, Geol. Soc. Lond. Spec. Publ., 191, 97–113, https://doi.org/10.1144/GSL.SP.2002.191.01.07, 2002.

Calle, M., Calle, J., Alho, P., and Benito, G.: Inferring sediment transfers and functional connectivity of rivers from repeat topographic surveys, Earth Surf. Process. Landf., 45, 681–693, https://doi.org/10.1002/esp.4765, 2020.

Church, M.: Bed Material Transport and the Morphology of Alluvial River Channels, Annu. Rev. Earth Planet. Sci., 34, 325–354, https://doi.org/10.1146/annurev.earth.33.092203.122721, 2006.

Church, M. and Haschenburger, J. K.: What is the "active layer"?, Water Resour. Res., 53, 5–10, https://doi.org/10.1002/2016WR019675, 2017.

Dragomiretskiy, K. and Zosso, D.: Variational Mode Decomposition, IEEE Trans. Signal Process., 62, 531–544, https://doi.org/10.1109/TSP.2013.2288675, 2014.

Ferguson, R. I. and Ashworth, P. J.: Spatial patterns of bedload transport and channel change in braided and near-braided rivers, Dyn. Gravel-Bed Rivers Billi P Hey RD Thorne CR Tacconi P Eds, 1992.

Garcia Lugo, G. A., Bertoldi, W., Henshaw, A. J., and Gurnell, A. M.: The effect of lateral confinement on gravel bed river morphology, Water Resour. Res., 51, 7145–7158, https://doi.org/10.1002/2015WR017081, 2015.

Goff, J. R. and Ashmore, P.: Gravel transport and morphological change in braided sunwapta river, Alberta, Canada, Earth Surf. Process. Landf., 19, 195–212, https://doi.org/10.1002/esp.3290190302, 1994.

Grams, P. E., Topping, D. J., Schmidt, J. C., Hazel Jr., J. E., and Kaplinski, M.: Linking morphodynamic response with sediment mass balance on the Colorado River in Marble Canyon: Issues of scale, geomorphic setting, and sampling design, J. Geophys. Res. Earth Surf., 118, 361–381, https://doi.org/10.1002/jgrf.20050, 2013.

Grams, P. E., Buscombe, D., Topping, D. J., Kaplinski, M., and Hazel, J. E.: How many measurements are required to construct an accurate sand budget in a large river? Insights from analyses of signal and noise, Earth Surf. Process. Landf., 44, 160–178, https://doi.org/10.1002/esp.4489, 2019.

Hassan, M. A. and Bradley, D. N.: Geomorphic Controls on Tracer Particle Dispersion in Gravel-Bed Rivers, in: Gravel-Bed Rivers, John Wiley & Sons, Ltd, 159–184, https://doi.org/10.1002/9781118971437.ch6, 2017.

Hassan, M. A., Church, M., and Schick, A. P.: Distance of movement of coarse particles in gravel bed streams, Water Resour. Res., 27, 503–511, https://doi.org/10.1029/90WR02762, 1991.

Hassan, M. A., Church, M., and Ashworth, P. J.: Virtual rate and mean distance of travel of individual clasts in gravel-bed channels, Earth Surf. Process. Landf., 17, 617–627, https://doi.org/10.1002/esp.3290170607, 1992.

Hoey, T.: Temporal variations in bedload transport rates and sediment storage in gravel-bed rivers, Prog. Phys. Geogr. Earth Environ., 16, 319–338, https://doi.org/10.1177/030913339201600303, 1992.

Huang, N., Chen, H., Cai, G., Fang, L., and Wang, Y.: Mechanical Fault Diagnosis of High Voltage Circuit Breakers Based on Variational Mode Decomposition and Multi-Layer Classifier, Sensors, 16, 1887, https://doi.org/10.3390/s16111887, 2016.

Inc, T. M.: MATLAB version: 9.13.0 (R2022b), 2022.

Kasprak, A., Wheaton, J. M., Ashmore, P. E., Hensleigh, J. W., and Peirce, S.: The relationship between particle travel distance and channel morphology: results from physical models of braided rivers., J. Geophys. Res. Earth Surf., 120, 55–74, 2015.

Lane, S. N., Richards, K. S., and Chandler, J. H.: Morphological Estimation of the Time-Integrated Bed Load Transport Rate, Water Resour. Res., 31, 761–772, https://doi.org/10.1029/94WR01726, 1995.

Lane, S. N., Westaway, R. M., and Murray Hicks, D.: Estimation of erosion and deposition volumes in a large, gravel-bed, braided river using synoptic remote sensing, Earth Surf. Process. Landf., 28, 249–271, https://doi.org/10.1002/esp.483, 2003.

Liébault, F., Bellot, H., Chapuis, M., Klotz, S., and Deschâtres, M.: Bedload tracing in a high-sediment-load mountain stream: BEDLOAD TRACING IN A HIGH-SEDIMENT-LOAD MOUNTAIN STREAM, Earth Surf. Process. Landf., 37, 385–399, https://doi.org/10.1002/esp.2245, 2012.

Lindsay, J. B. and Ashmore, P. E.: The effects of survey frequency on estimates of scour and fill in a braided river model, Earth Surf. Process. Landf., 27, 27–43, https://doi.org/10.1002/esp.282, 2002.

Liu, S., He, Q., Gao, R. X., and Freedson, P.: Empirical mode decomposition applied to tissue artifact removal from respiratory signal, in: 2008 30th Annual International Conference of the IEEE Engineering in Medicine and Biology Society, 2008 30th Annual International Conference of the IEEE Engineering in Medicine and Biology Society, 3624–3627, https://doi.org/10.1109/IEMBS.2008.4649991, 2008.

Ma, W., Yin, S., Jiang, C., and Zhang, Y.: Variational mode decomposition denoising combined with the Hausdorff distance, Rev. Sci. Instrum., 88, 035109, https://doi.org/10.1063/1.4978029, 2017.

Mao, L., Picco, L., Lenzi, M. A., and Surian, N.: Bed material transport estimate in large gravel-bed rivers using the virtual velocity approach: Virtual velocity for bed material transport estimate, Earth Surf. Process. Landf., 42, 595–611, https://doi.org/10.1002/esp.4000, 2017.

McDowell, C. and Hassan, M. A.: The influence of channel morphology on bedload path lengths: Insights from a survival process model, Earth Surf. Process. Landf., 45, 2982–2997, https://doi.org/10.1002/esp.4946, 2020.

McDowell, C., Gaeuman, D., and Hassan, M. A.: Linkages between bedload displacements and topographic change, Earth Surf. Process. Landf., 46, 3127–3142, https://doi.org/10.1002/esp.5221, 2021.

805   McLean, D. G. and Church, M.: Sediment transport along lower Fraser River: 2. Estimates based on
806   the long-term gravel budget, Water Resour. Res., 35, 2549–2559,
807   https://doi.org/10.1029/1999WR900102, 1999.

808   McQueen, R., Ashmore, P., Millard, T., and Goeller, N.: Bed Particle Displacements and
809   Morphological Development in a Wandering Gravel-Bed River, Water Resour. Res., 57,
810   https://doi.org/10.1029/2020WR027850, 2021.

811   Montgomery, D. R. and Buffington, J. M.: Channel-reach morphology in mountain drainage basins,
812   GSA Bull., 109, 596–611, https://doi.org/10.1130/0016-7606(1997)109<0596:CRMIMD>2.3.CO;2,
813   1997.

814   Pyrce, R. and Ashmore, P.: The relation between particle path length distributions and channel
815   morphology in gravel-bed streams: A synthesis, Geomorphology, 56, 167–187,
816   https://doi.org/10.1016/S0169-555X(03)00077-1, 2003a.

817   Pyrce, R. S. and Ashmore, P. E.: Particle path length distributions in meandering gravel-bed
818   streams: results from physical models, Earth Surf. Process. Landf., 28, 951–966,
819   https://doi.org/10.1002/esp.498, 2003b.

820   Pyrce, R. S. and Ashmore, P. E.: Bedload path length and point bar development in gravel-bed river
821   models, Sedimentology, 52, 839–857, https://doi.org/10.1111/j.1365-3091.2005.00714.x, 2005.

822   Redolfi, M.: Sediment transport and morphology of braided rivers: steady and unsteady regime, n.d.

823   Roux, C., Alber, A., Bertrand, M., Vaudor, L., and Piégay, H.: "FluvialCorridor": A new ArcGIS
824   toolbox package for multiscale riverscape exploration, Geomorphology, 242, 29–37,
825   https://doi.org/10.1016/j.geomorph.2014.04.018, 2015.

826   Schneider, J. M., Turowski, J. M., Rickenmann, D., Hegglin, R., Arrigo, S., Mao, L., and Kirchner,
827   J. W.: Scaling relationships between bed load volumes, transport distances, and stream power in
828   steep mountain channels, J. Geophys. Res. Earth Surf., 119, 533–549,
829   https://doi.org/10.1002/2013JF002874, 2014.

830   Sigmund, M.: Voice Recognition by Computer, Tectum Verlag DE, 114 pp., 2003.

831   Upadhyay, A. and Pachori, R. B.: Instantaneous voiced/non-voiced detection in speech signals
832   based on variational mode decomposition, J. Frankl. Inst., 352, 2679–2707,
833   https://doi.org/10.1016/j.jfranklin.2015.04.001, 2015.

834   Vázquez-Tarrío, D. and Batalla, R. J.: Assessing Controls on the Displacement of Tracers in
835   Gravel-Bed Rivers, Water, 11, 1598, https://doi.org/10.3390/w11081598, 2019.

836   Vázquez-Tarrío, D., Recking, A., Liébault, F., Tal, M., and Menéndez-Duarte, R.: Particle transport
837   in gravel-bed rivers: Revisiting passive tracer data: Particle transport in gravel-bed rivers, Earth
838   Surf. Process. Landf., 44, 112–128, https://doi.org/10.1002/esp.4484, 2019.

839   Vericat, D., Wheaton, J. M., and Brasington, J.: Revisiting the Morphological Approach, in: Gravel-
840   Bed Rivers, John Wiley & Sons, Ltd, 121–158, https://doi.org/10.1002/9781118971437.ch5, 2017.

841   Wheaton, J. M.: Uncertainity in morphological sediment budgeting of rivers, phd, University of
842   Southampton, 2008.

843   Wheaton, J. M., Brasington, J., Darby, S. E., and Sear, D. A.: Accounting for uncertainty in DEMs
844   from repeat topographic surveys: improved sediment budgets, Earth Surf. Process. Landf., 35, 136–
845   156, https://doi.org/10.1002/esp.1886, 2010.

846   Wilcock, P. R.: Entrainment, displacement and transport of tracer gravels, Earth Surf. Process.
847   Landf., 22, 1125–1138, https://doi.org/10.1002/(SICI)1096-9837(199712)22:12<1125::AID-
848   ESP811>3.0.CO;2-V, 1997.

849   Wu, S., Feng, F., Zhu, J., Wu, C., and Zhang, G.: A Method for Determining Intrinsic Mode
850   Function Number in Variational Mode Decomposition and Its Application to Bearing Vibration
851   Signal Processing, Shock Vib., 2020, 1–16, https://doi.org/10.1155/2020/8304903, 2020.

852